

CISSIR: Beam Codebooks with Self-Interference Reduction Guarantees for Integrated Sensing and Communication Beyond 5G

Rodrigo Hernangómez, *Member, IEEE*, Jochen Fink, *Member, IEEE*,
Renato Luís Garrido Cavalcante, *Member, IEEE*, and Sławomir Stańczak, *Senior Member, IEEE*

Abstract—We propose a beam codebook design to reduce self-interference (SI) in integrated sensing and communication (ISAC) systems. Our optimization methods, which can be applied to both tapered beamforming and phased arrays, adapt the codebooks to the SI channel such that a certain SI level is achieved. Furthermore, we derive an upper bound on the quantization noise in terms of the achieved SI level, which provides guidelines to pose the optimization problem in order to obtain performance guarantees for sensing. By selecting standard reference codebooks in our simulations, we show substantially improved sensing quality with little impact on 5G-NR communication. Our proposed method is not only less dependent on hyperparameters than other approaches in the literature, but it can also reduce SI further, and thus deliver better sensing and communication performance.

Index Terms—Integrated sensing and communication, beamforming, phased arrays, self-interference

I. INTRODUCTION

NEXT-GENERATION mobile networks are expected to incorporate sensing capabilities as an additional service [1]. To this aim, the paradigm of integrated sensing and communication (ISAC) is being actively investigated, and ISAC’s many challenges and opportunities are rapidly unfolding as a result [2]–[4].

Self-interference (SI) has been identified as one such ISAC challenge, principally, but not only, in so-called monostatic setups with co-located transmission (TX) and reception (RX) sensing systems [4]–[6]. Whereas conventional radar typically achieves TX-RX isolation by discarding RX echoes that overlap with the TX signals on the time-frequency plane [7], ISAC signals are often dense in time and frequency in order to satisfy communication requirements. Consequently, self-interference produces an unwanted signal contribution at the ISAC receiver, causing adverse effects at different stages: at the RX antenna (saturation), the analog-to-digital converter (ADC) (desensitization), or the digital baseband (signal masking) [8], [9]. The former stages are critical due to the nonlinear distortion they may introduce, hence a cascaded approach is often adopted such that different SI thresholds are attained at each analog stage to avoid distortion, and the residual SI is canceled via digital signal processing [7], [8].

The problem of SI has been addressed through many different strategies, including reactive decoupling [9], active

cancelers [10], beamforming [11]–[17], or intelligent reflecting surfaces [18]. From the perspective of mobile networks, beamforming is perhaps the most practical approach, since it is already an integral part of 5G new radio (NR) standards together with multiple-input multiple-output (MIMO) processing [19]. Since digital RX beamforming fails to address all effects happening before the ADC [11], analog [12]–[15] and hybrid [16], [17] architectures represent a more natural choice.

5G-NR MIMO/beamforming typically operates via predefined codebooks under limited channel state information (CSI) [19]. The authors of [14], [15] have proposed methods for designing codebooks that achieve considerably lower SI than 5G-NR codebooks. However, they rely on hyperparameter tuning and heuristic optimization. Moreover, these methods are devised with the assumption of flat-fading SI channels. In contrast to this, radio measurements and industrial applications often deal with multipath SI channels, whereby strong clutter reflections are as relevant as direct antenna coupling despite the longer propagation path [20]–[22].

In this paper, we propose a principled SI-reduced beam codebook design method for ISAC, which we call CISSIR¹. For this, we adopt the system model in Section II, which considers realistic multipath MIMO SI channels and is general enough to cover analog and hybrid codebooks, either based on tapered beamforming or on phased arrays. In Section III, we develop optimization frameworks using matrix decomposition, for tapered beamforming, and semidefinite programming (SDP), for phased arrays [23]. At the same time, we establish in Section IV an analytical bound on ADC quantization error with respect to SI power, from which we extract guidelines to select optimization parameters such that sensing constraints are met. By doing so, we provide codebooks with integral split for self-interference reduction (CISSIR) with feasibility and performance guarantees. The simulations in Section V, implemented with SionnaTM [24], illustrate the analytically-derived performance guarantees and showcase the merits of CISSIR in comparison to the LoneSTAR codebook [14]. Last but not least, link-level simulations confirm CISSIR compatibility with the 5G NR standard.

A. Notation and preliminaries

We denote the positive integers with \mathbb{N}_+ , and we define $[N] := \{1, 2, \dots, N\}$ with $N \in \mathbb{N}_+$. For $z \in \mathbb{C}$, we indicate

¹Pronounced like “scissor”. Code available at github.com/rodrihgh/cissir.

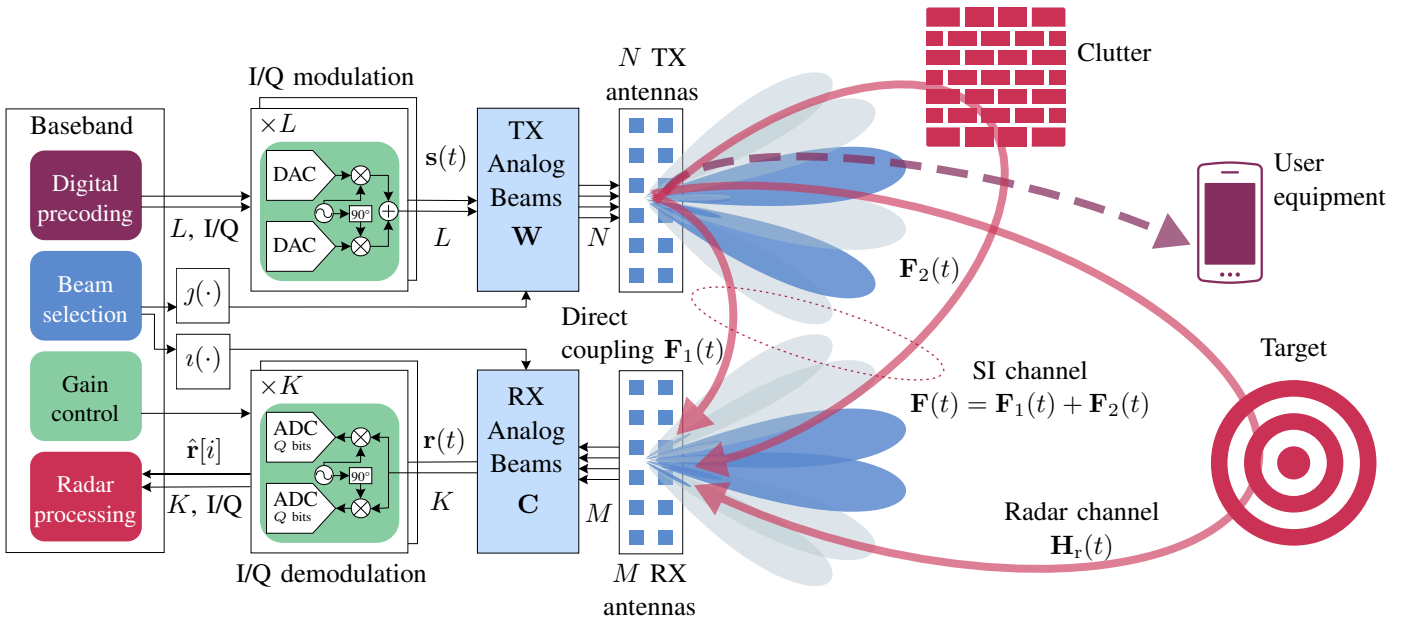


Fig. 1. System model: ISAC beam codebooks in the face of self-interference (SI). Amplifiers and filters are omitted for simplicity.

its real and imaginary parts as $\Re(z)$ and $\Im(z)$, respectively, and its conjugate as $z^* = \Re(z) - j\Im(z)$ with $j = \sqrt{-1}$.

We write $\mathcal{CN}(0, \sigma^2)$ to denote the zero-mean complex normal distribution with variance σ^2 , and $\mathcal{U}(a, b)$ for the uniform distribution in $[a, b]$. The expected value of a random variable X is written as $\mathbb{E}[X]$.

Uppercase bold letters represent matrices $\mathbf{V} \in \mathbb{C}^{M \times N}$, with subindexed lowercase bold letters indicating their column vectors, $\mathbf{V} = [\mathbf{v}_1, \dots, \mathbf{v}_N]$, ($\forall n \in [N]$) $\mathbf{v}_n \in \mathbb{C}^M$. We write the convolution of functions $f: \mathbb{R} \rightarrow \mathbb{C}$ and $g: \mathbb{R} \rightarrow \mathbb{C}$ as $f * g$. For $p \in [1, \infty]$, the p -norm for vectors $\mathbf{v} \in \mathbb{C}^M$ is written as $\|\mathbf{v}\|_p$, whereas $|f|_p$ denotes the p -norm for functions ($\forall a, b \in \mathbb{R}$ and $a < b$) $f: [a, b] \rightarrow \mathbb{C}$, to avoid confusion. Moreover, $\|\mathbf{M}\|_F$, $\|\mathbf{M}\|_2$, and $\|\mathbf{M}\|_*$ indicate the Frobenius, spectral, and nuclear norms, respectively, of $\mathbf{M} \in \mathbb{C}^{M \times N}$. For any matrix $\mathbf{A} \in \mathbb{C}^{M \times N}$, we write its transpose as \mathbf{A}^T and its Hermitian transpose as $\mathbf{A}^H = (\mathbf{A}^*)^T$. For a matrix-valued function $\mathbf{F}: \mathbb{R} \rightarrow \mathbb{C}^{M \times N}$, $\mathbf{u} \in \mathbb{C}^M$, and $\mathbf{v} \in \mathbb{C}^N$, $(\mathbf{u}^H \mathbf{F} \mathbf{v})(t)$ stands for the function $t \mapsto \mathbf{u}^H \mathbf{F}(t) \mathbf{v}$, and the integral of $\mathbf{F}(t)$ is understood entry-wise, i.e. ($\forall n \in [N]$, $\forall m \in [M]$):

$$\left[\int_{t_0}^{t_1} \mathbf{F}(t) dt \right]_{m,n} = \int_{t_0}^{t_1} [\mathbf{F}(t)]_{m,n} dt.$$

For any pair of Hermitian matrices $\mathbf{A}, \mathbf{B} \in \mathbb{S}^M := \{\mathbf{X} \in \mathbb{C}^{M \times M} \mid \mathbf{X} = \mathbf{X}^H\}$, we consider the inner product $\langle \mathbf{A}, \mathbf{B} \rangle := \text{tr}(\mathbf{B}^H \mathbf{A}) = \text{tr}(\mathbf{B} \mathbf{A}) \in \mathbb{R}$. We denote by $\mathbb{S}_+^M \subset \mathbb{S}^M$ the $M \times M$ positive semidefinite (PSD) cone, which induces the partial order ($\forall \mathbf{A}, \mathbf{B} \in \mathbb{S}^M$) $\mathbf{A} \succcurlyeq \mathbf{B} \iff \mathbf{A} - \mathbf{B} \in \mathbb{S}_+^M$.

II. SYSTEM MODEL AND PROBLEM FORMULATION

A. System model

We consider a hybrid-beamforming MIMO system with N TX antennas and $L < N$ TX radio frequency (RF) chains, as depicted in Fig. 1. For a given time slot of length T , the TX

RF chains are fed with L time-continuous signals, which we write in vector form ($\forall t \in [0, T]$) as $\mathbf{s}(t) := [s_1(t), \dots, s_L(t)]$ with ($\forall \ell \in [L]$) $s_\ell: [0, T] \rightarrow \mathbb{C}$.

The signals in $\mathbf{s}(t)$ carry user data and are transmitted according to L selected beamforming vectors out of $L' \geq L$ columns from a given TX codebook matrix $\mathbf{W} \in \mathbb{C}^{N \times L'}$. Beam selection is determined by a mapping $j: [L] \rightarrow [L']$, so that ($\forall \ell \in [L]$) the beamformer $\mathbf{w}_{j(\ell)}$ is applied to $s_\ell(t)$.

Likewise, the system has an RX side that is dedicated to radar sensing and equipped with M antennas and K RF chains. The k -th RX signal is beamformed ($\forall k \in [K]$) by $\mathbf{c}_{i(k)}$, a vector selected from the $K' \geq K$ columns in the RX codebook $\mathbf{C} \in \mathbb{C}^{M \times K'}$ according to $i: [K] \rightarrow [K']$.

The TX and RX codebooks are restricted to the feasibility sets $\mathcal{W}^{L'}$ and $\mathcal{C}^{K'}$, i.e.:

$$\begin{aligned} \mathcal{W} \in \mathcal{W}^{L'} &:= \left\{ \mathbf{W} \in \mathbb{C}^{N \times L'} \mid (\forall \ell \in [L']) \mathbf{w}_\ell \in \mathcal{W} \right\}, \\ \mathcal{C} \in \mathcal{C}^{K'} &:= \left\{ \mathbf{C} \in \mathbb{C}^{M \times K'} \mid (\forall k \in [K']) \mathbf{c}_k \in \mathcal{C} \right\}, \end{aligned}$$

where $\mathcal{W} \in \{\mathcal{W}_b, \mathcal{W}_\circ\}$ and $\mathcal{C} \in \{\mathcal{C}_b, \mathcal{C}_\circ\}$ express certain beamforming constraints. In the case of tapered beamforming, the codebook columns are only subject to unit power:

$$\mathcal{W}_b := \{\mathbf{w} \in \mathbb{C}^N \mid \|\mathbf{w}\|_2 = 1\}, \quad \mathcal{C}_b := \{\mathbf{c} \in \mathbb{C}^M \mid \|\mathbf{c}\|_2 = 1\}. \quad (1)$$

On the other hand, for phased arrays we have

$$\begin{aligned} \mathcal{W}_\circ &:= \left\{ \mathbf{w} \in \mathbb{C}^N \mid (\forall n \in [N]) \ |[\mathbf{w}]_n| = 1/\sqrt{N} \right\}, \\ \mathcal{C}_\circ &:= \left\{ \mathbf{c} \in \mathbb{C}^M \mid (\forall m \in [M]) \ |[\mathbf{c}]_m| = 1/\sqrt{M} \right\}. \end{aligned}$$

We note that $\mathcal{W}_\circ \subset \mathcal{W}_b$ and $\mathcal{C}_\circ \subset \mathcal{C}_b$, i.e., beam unit power is assumed for both beamforming variants.

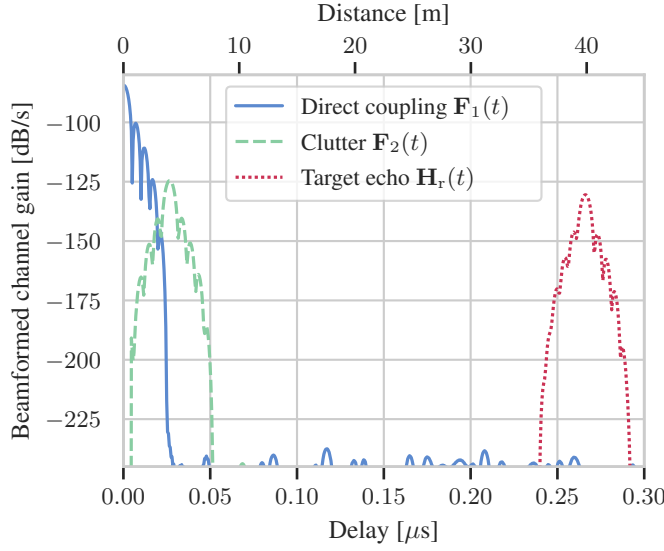


Fig. 2. Power delay profile of a beamformed channel pointing towards a target at -39° . The contributions from $\mathbf{F}_1(t)$, $\mathbf{F}_2(t)$, and $\mathbf{H}_r(t)$ are highlighted with different colors.

The signals in $\mathbf{s}(t)$ impinge on the RX sensing side over a MIMO channel $\mathbf{H} : [0, T_c] \rightarrow \mathbb{C}^{M \times N}$ with maximum delay T_c , which we write ($\forall t \in [0, T_c], \forall m \in [M], \forall n \in [N]$) as:

$$\mathbf{H}(t) := \begin{bmatrix} h_{1,1}(t) & \dots & h_{1,N}(t) \\ \vdots & \ddots & \vdots \\ h_{M,1}(t) & \dots & h_{M,N}(t) \end{bmatrix}, \quad h_{m,n} : [0, T_c] \rightarrow \mathbb{C}. \quad (2)$$

Furthermore, we assume $\mathbf{H}(t)$ to be the superimposition of the unknown radar channel $\mathbf{H}_r : [0, T_c] \rightarrow \mathbb{C}^{M \times N}$ and the SI channel $\mathbf{F} : [0, T_c] \rightarrow \mathbb{C}^{M \times N}$:

$$(\forall t \in [0, T_c]) \quad \mathbf{H}(t) = \mathbf{H}_r(t) + \mathbf{F}(t) = \mathbf{H}_r(t) + \sum_{d=1}^D \mathbf{F}_d(t),$$

where $\mathbf{F}(t)$ is known through calibration and is composed of D paths ($\forall d \in [D]$) $\mathbf{F}_d : [0, T_c] \rightarrow \mathbb{C}^{M \times N}$ (e.g., direct antenna coupling $\mathbf{F}_1(t)$ and clutter reflection $\mathbf{F}_2(t)$ in Fig. 1). Similarly to the entries of $\mathbf{H}(t)$ in (2), all entries in $\mathbf{H}_r(t)$ and $\mathbf{F}(t)$ are also functions with domain in $[0, T_c]$. Any $\mathbf{c} \in \mathcal{C}$ and $\mathbf{w} \in \mathcal{W}$ yield a *beamformed channel* $\mathbf{c}^H \mathbf{H} \mathbf{w} : [0, T_c] \rightarrow \mathbb{C}$, like the example in Fig. 2, which is used for simulations in Section V.

The RX signals are expressed in vector form as $\mathbf{r}(t)$:

$$(\forall t \in [0, T + T_c]) \quad \mathbf{r}(t) = [r_1(t), \dots, r_K(t)]^\top, \quad \text{where} \\ (\forall k \in [K]) \quad r_k(t) = \sum_{\ell=1}^L \left(\left(\mathbf{c}_{i(k)}^H \mathbf{H} \mathbf{w}_{j(\ell)} \right) * s_\ell \right) (t). \quad (3)$$

For all $k \in [K]$, two ADCs sample the in-phase/quadrature (I/Q) components of $r_k(t)$ at the rate $1/T_S$ with Q quantization

bits each, yielding the following RX digital sensing signal ($\forall i \in \{0, 1, \dots, \lfloor (T + T_c)/T_S \rfloor\}$):

$$\hat{\mathbf{r}}[i] = [\hat{r}_1[i], \dots, \hat{r}_K[i]]^\top, \\ (\forall k \in [K]) \quad \hat{r}_k[i] := r_k(iT_S) + v_k[i] + u_k[i]. \quad (4)$$

In (4), $v_k[i] \sim \mathcal{CN}(0, \sigma_v^2)$ is a sample of independent identically distributed (i.i.d.) thermal noise, whereas $u_k[i]$ is a sample of complex quantization noise. The latter is described in more detail in Section IV.

B. The optimization problem

Wireless communication systems employ TX and RX beam codebooks, $\mathbf{Y} \in \mathcal{W}^{L'}$ and $\mathbf{Z} \in \mathcal{C}^{K'}$, that are typically designed for time- or frequency-division duplex without taking the SI channel $\mathbf{F}(t)$ into account [19]. In ISAC systems, however, SI may decrease sensing performance dramatically [4]–[6]. For this reason, some authors design $\mathbf{W} \in \mathcal{W}^{L'}$ and $\mathbf{C} \in \mathcal{C}^{K'}$ in Fig. 1 to minimize some SI-related quantity, while they impose a maximum deviation between (\mathbf{W}, \mathbf{C}) and the reference codebooks (\mathbf{Y}, \mathbf{Z}) to limit communication impairment [14], [15]. In contrast to this, we suggest minimizing the distance between reference and optimized codebooks under a constraint on the *maximum SI (max. SI)* $\mathfrak{m}_{\mathbf{F}}(\mathbf{C}, \mathbf{W})$, which we define for $\mathbf{F}(t)$ ($\forall \mathbf{C} \in \mathcal{C}^{K'}, \forall \mathbf{W} \in \mathcal{W}^{L'}$) to be:

$$\mathfrak{m}_{\mathbf{F}}(\mathbf{C}, \mathbf{W}) := \max_{\substack{k \in [K'], \\ \ell \in [L']}} \int_0^{T_c} |\mathbf{c}_k^H \mathbf{F}(t) \mathbf{w}_\ell| dt. \quad (5)$$

The max. SI constraint allows us to upper bound the RX noise of $\hat{\mathbf{r}}[i]$ in (4), as we discuss in Section IV. We note that (5) does not depend on the TX signal $\mathbf{s}(t)$ or the beam-selection mappings $i(\cdot)$ and $j(\cdot)$, since these may be unknown during codebook design.

In line with the literature, we use the Frobenius norm to assess the distance between reference and optimized codebooks. That is, we aim to minimize the TX and RX codebook deviation, σ_{tx}^2 and σ_{rx}^2 , defined as:

$$\sigma_{\text{tx}}^2 := \|\mathbf{W} - \mathbf{Y}\|_{\text{F}}^2 / \|\mathbf{Y}\|_{\text{F}}^2 = \frac{1}{L'} \sum_{\ell=1}^{L'} \|\mathbf{w}_\ell - \mathbf{y}_\ell\|_2^2, \\ \sigma_{\text{rx}}^2 := \|\mathbf{C} - \mathbf{Z}\|_{\text{F}}^2 / \|\mathbf{Z}\|_{\text{F}}^2 = \frac{1}{K'} \sum_{k=1}^{K'} \|\mathbf{c}_k - \mathbf{z}_k\|_2^2, \quad (6)$$

such that the max. SI $\mathfrak{m}_{\mathbf{F}}(\mathbf{C}, \mathbf{W})$ does not exceed a given *target SI* $\varepsilon > 0$. The optimization problem to solve is thus

$$\underset{\mathbf{W} \in \mathcal{W}^{L'}, \mathbf{C} \in \mathcal{C}^{K'}}{\text{minimize}} \quad \|\mathbf{W} - \mathbf{Y}\|_{\text{F}}^2 + \omega \|\mathbf{C} - \mathbf{Z}\|_{\text{F}}^2 \quad (7a)$$

$$\text{s.t.} \quad \mathfrak{m}_{\mathbf{F}}(\mathbf{C}, \mathbf{W}) \leq \varepsilon, \quad (7b)$$

with $\omega > 0$ a trade-off parameter between TX and RX codebook deviation.

III. PROPOSED SCHEME

Problem (7) is nonconvex due to the constraint (1) embedded in the sets $\mathcal{C}^{K'}$ and $\mathcal{W}^{L'}$, and also due to the coupling of \mathbf{C} and \mathbf{W} in $\mathfrak{m}_{\mathbf{F}}(\mathbf{C}, \mathbf{W})$. In order to derive a more tractable

problem, we propose a decoupling of the codebooks \mathbf{C} and \mathbf{W} . The resulting problem, albeit still nonconvex, can be solved optimally for the case of tapered beamforming and phased arrays, as we detail in Sections III-B–III-C.

A. Problem decoupling

We propose an alternative to Problem (7) that allows us to optimize the columns of \mathbf{C} and \mathbf{W} individually while (\mathbf{C}, \mathbf{W}) remains in the original feasible region. For this, we consider an *integral split* of the SI channel to “decouple” \mathbf{C} and \mathbf{W} .

Definition 1 (Integral split). We define the integral split of an SI channel $\mathbf{F}(t)$ as the matrices $\mathbf{G}_{\text{tx}} \in \mathbb{S}_+^N$ and $\mathbf{G}_{\text{rx}} \in \mathbb{S}_+^M$:

$$\mathbf{G}_{\text{tx}} := \int_0^{T_c} \mathbf{V}_t \boldsymbol{\Sigma}_t \mathbf{V}_t^H dt, \text{ and } \mathbf{G}_{\text{rx}} := \int_0^{T_c} \mathbf{U}_t \boldsymbol{\Sigma}_t \mathbf{U}_t^H dt,$$

where, for every $t \in [0, T_c]$, \mathbf{U}_t , $\boldsymbol{\Sigma}_t$, and \mathbf{V}_t^H are given as a singular value decomposition (SVD) of $\mathbf{F}(t) = \mathbf{U}_t \boldsymbol{\Sigma}_t \mathbf{V}_t^H$.

Using the integral split of $\mathbf{F}(t)$, we propose obtaining the columns of $\mathbf{W} = [\mathbf{w}_1, \dots, \mathbf{w}_{L'}]$ and $\mathbf{C} = [\mathbf{c}_1, \dots, \mathbf{c}_{K'}]$ as the solutions to $L' + K'$ problems in the following form:

$$\underset{\mathbf{x} \in \mathbb{C}^P}{\text{maximize}} \quad \Re(\mathbf{b}^H \mathbf{x}) \quad (8a)$$

$$\text{s.t.} \quad \mathbf{x}^H \mathbf{G} \mathbf{x} \leq \epsilon, \quad (8b)$$

$$\mathbf{x} \in \mathcal{X}, \quad (8c)$$

with the parameters $P \in \mathbb{N}_+$, $\mathcal{X} \subset \mathbb{C}^P$, $\mathbf{b} \in \mathcal{X}$, $\mathbf{G} \in \mathbb{S}_+^P$, and $\epsilon > 0$ chosen $\forall \ell \in [L']$, $\forall k \in [K']$ as

$$\begin{aligned} P = N, \mathcal{X} = \mathcal{W}, \mathbf{b} = \mathbf{y}_\ell, \mathbf{G} = \mathbf{G}_{\text{tx}}, \epsilon = \epsilon^\beta, \text{ for } \mathbf{w}_\ell, \\ P = M, \mathcal{X} = \mathcal{C}, \mathbf{b} = \mathbf{z}_k, \mathbf{G} = \mathbf{G}_{\text{rx}}, \epsilon = \epsilon^{2-\beta}, \text{ for } \mathbf{c}_k, \end{aligned} \quad (9)$$

for $\epsilon > 0$ in (7) and $\beta \in [0, 2]$. The proposed approach in (8)–(9), although not equivalent to the original optimization problem (7), is related to it via the next proposition.

Proposition 1. Let $\mathbf{G}_{\text{tx}} \in \mathbb{S}_+^N$ and $\mathbf{G}_{\text{rx}} \in \mathbb{S}_+^M$ be the integral split (Definition 1) of $\mathbf{F}(t)$ in (5), and consider the quantity:

$$\mathfrak{s}_{\mathbf{F}}(\mathbf{C}, \mathbf{W}) := \max_{k \in [K']} \sqrt{\mathbf{c}_k^H \mathbf{G}_{\text{rx}} \mathbf{c}_k} \max_{\ell \in [L']} \sqrt{\mathbf{w}_\ell^H \mathbf{G}_{\text{tx}} \mathbf{w}_\ell}. \quad (10)$$

Then, each of the following holds:

i) Replacing $\mathfrak{m}_{\mathbf{F}}(\mathbf{C}, \mathbf{W})$ with $\mathfrak{s}_{\mathbf{F}}(\mathbf{C}, \mathbf{W})$ in (7b) yields a restriction of Problem (7), such that the feasible points of this restricted problem are also feasible for (7) by

$$(\forall \mathbf{C} \in \mathcal{C}^{K'}, \forall \mathbf{W} \in \mathcal{W}^{L'}) \mathfrak{m}_{\mathbf{F}}(\mathbf{C}, \mathbf{W}) \leq \mathfrak{s}_{\mathbf{F}}(\mathbf{C}, \mathbf{W}) \leq \epsilon. \quad (11)$$

ii) A solution to this restricted problem, $\mathbf{W} \in \mathcal{W}^{L'}$ and $\mathbf{C} \in \mathcal{C}^{K'}$, can be obtained column-wise ($\forall \ell \in [L']$, $\forall k \in [K']$) as solutions to (8) under the parametrizations in (9).

Proof. The proof is given in Appendix A. \square

We point out that the codebooks obtained through (8)–(9) are not a solution to Problem (7) in general, due to the restriction (11). Nevertheless, in Section V we show empirically that in fact $\mathfrak{m}_{\mathbf{F}}(\mathbf{C}, \mathbf{W}) \approx \mathfrak{s}_{\mathbf{F}}(\mathbf{C}, \mathbf{W})$ for some practical scenarios. We also note that the original TX/RX

weight parameter ω in (7) disappears in our proposed scheme due to the column separation, but we can use β in (9) instead to trade off TX and RX codebook deviation. More information on how to choose ϵ and β is provided in Section IV.

We refer to the solutions to (8)–(9) as *codebooks with integral split for self-interference reduction (CISSIR)*. In the following Sections III-B–III-C, we particularize Problem (8) for specific choices of \mathcal{C} and \mathcal{W} , but we first remark some general properties induced by the unit power constraint (1) from our system model in Section II-A.

Remark 1. Problem (8) is still nonconvex for $\mathcal{X} \in \{\mathcal{W}_\triangleright, \mathcal{W}_\circ, \mathcal{C}_\triangleright, \mathcal{C}_\circ\}$ due to (1). A straightforward convex relaxation can be obtained by replacing \mathcal{X} with its convex hull.

Remark 2. The optimal value of Problem (8) is upper bounded by 1, and it is attained with $\mathbf{x}_* = \mathbf{b}$ if $\epsilon \geq \mathbf{b}^H \mathbf{G} \mathbf{b}$. To see this, we note that, $\forall \mathbf{x}_* \in \mathcal{X}$, we have:

$$\Re(\mathbf{b}^H \mathbf{x}_*) \leq |\mathbf{b}^H \mathbf{x}_*| \leq \|\mathbf{b}\|_2 \|\mathbf{x}_*\|_2 = 1,$$

where the equality follows from (1). The inequalities above become tight for $\mathbf{x}_* = \mathbf{b}$, but \mathbf{b} is only feasible if $\epsilon \geq \mathbf{b}^H \mathbf{G} \mathbf{b}$.

B. Tapered beamforming

We first particularize Problem (8) to tapered beamforming, such that amplitude and phase can be controlled continuously and individually for every antenna element. As we will see, this case admits a semi-closed form solution that relies only on matrix decompositions and other linear algebra operations.

For tapering, we have $\mathcal{W} = \mathcal{W}_\triangleright$ and $\mathcal{C} = \mathcal{C}_\triangleright$, and Problem (8) takes the form:

$$\underset{\mathbf{x} \in \mathbb{C}^P}{\text{maximize}} \quad \Re(\mathbf{b}^H \mathbf{x}) \quad (12a)$$

$$\text{s.t.} \quad \mathbf{x}^H \mathbf{G} \mathbf{x} \leq \epsilon, \quad (12b)$$

$$\mathbf{x}^H \mathbf{x} = 1. \quad (12c)$$

Although Problem (12) is nonconvex, it can be solved efficiently as stated below and outlined in Algorithm 1.

Proposition 2. Consider a spectral decomposition $\mathbf{G} = \mathbf{Q} \boldsymbol{\Gamma} \mathbf{Q}^H$ of the matrix $\mathbf{G} \in \mathbb{S}_+^P$ in (12b), where \mathbf{Q} is unitary and $\boldsymbol{\Gamma}$ a diagonal matrix with diagonal entries given by ($\forall p \in [P]$) $\sigma_p := [\boldsymbol{\Gamma}]_{p,p}$. Problem (12) admits a solution

$$\begin{aligned} \mathbf{x}_* &= \check{\mathbf{x}} / \|\check{\mathbf{x}}\|_2, \quad \text{with } \check{\mathbf{x}} := \mathbf{Q} \mathbf{D}_{\nu_*} \mathbf{Q}^H \mathbf{b}, \\ \mathbf{D}_{\nu} &:= \text{diag} \left(\frac{1}{\sigma_1 + \nu}, \dots, \frac{1}{\sigma_P + \nu} \right), \end{aligned}$$

where ν_* is a positive root of the real polynomial

$$\mathcal{P}(\nu) := \sum_{p=1}^P (\sigma_p - \epsilon) |\mathbf{q}_p^H \mathbf{b}|^2 \prod_{q \neq p} (\sigma_q + \nu)^2,$$

if one of the following sufficient conditions is satisfied:

- i) $\text{rank}(\mathbf{G}) < P$ and $\epsilon \in (0, \mathbf{b}^H \mathbf{G} \mathbf{b})$, or
- ii) $\text{rank}(\mathbf{G}) = P$ and $\epsilon \in (\bar{\sigma}(\mathbf{b}, \mathbf{G}), \mathbf{b}^H \mathbf{G} \mathbf{b})$, with

$$\bar{\sigma}(\mathbf{b}, \mathbf{G}) := \frac{\sum_{p=1}^P \sigma_p |\mathbf{q}_p^H \mathbf{b}|^2 / \sigma_p^2}{\sum_{p=1}^P |\mathbf{q}_p^H \mathbf{b}|^2 / \sigma_p^2}.$$

Proof. The proof is given in Appendix B. \square

Algorithm 1 Tapered CISSIR optimization.

Require: $\mathbf{F}(t), \mathbf{Y}, \mathbf{Z}, \varepsilon, \beta$

- 1: $\mathbf{G}_{\text{tx}}, \mathbf{G}_{\text{rx}} \leftarrow \text{INTEGRALSPLIT}(\mathbf{F}(t))$ ▷ Def. 1
- 2: $\mathbf{W} \leftarrow \text{SPECTRALCODEBOOK}(\mathbf{Y}, \mathbf{G}_{\text{tx}}, \varepsilon^\beta)$
- 3: $\mathbf{C} \leftarrow \text{SPECTRALCODEBOOK}(\mathbf{Z}, \mathbf{G}_{\text{rx}}, \varepsilon^{2-\beta})$
- 4: **return** \mathbf{W}, \mathbf{C}
- 5: **function** $\text{SPECTRALCODEBOOK}(\mathbf{B}, \mathbf{G}, \varepsilon)$
- 6: $\mathbf{Q}, \mathbf{\Gamma} \leftarrow \text{SPECTRALDECOMPOSITION}(\mathbf{G})$ ▷ Prop. 2
- 7: **for** $r = 1, 2, \dots, R := \text{NUMCOLUMNS}(\mathbf{G})$ **do**
- 8: $\mathbf{b} \leftarrow [\mathbf{B}]_{:,r}$
- 9: **if** $\varepsilon < \mathbf{b}^H \mathbf{G} \mathbf{b}$ **then**
- 10: $\mathbf{x}_r \leftarrow \text{OPTIMIZEVECTOR}(\mathbf{b}, \varepsilon, \mathbf{Q}, \mathbf{\Gamma})$
- 11: **else**
- 12: $\mathbf{x}_r \leftarrow \mathbf{b}$
- 13: **end if**
- 14: **end for**
- 15: **return** $[\mathbf{x}_1, \mathbf{x}_2, \dots, \mathbf{x}_R]$
- 16: **end function**
- 17: **function** $\text{OPTIMIZEVECTOR}(\mathbf{b}, \varepsilon, \mathbf{Q}, \mathbf{\Gamma})$
- 18: $\mathcal{P}(\nu) \leftarrow \text{BUILDPOLY}(\mathbf{b}, \varepsilon, \mathbf{Q}, \mathbf{\Gamma})$ ▷ Prop. 2
- 19: $\nu_* \leftarrow \text{LARGESTREALROOT}(\mathcal{P}(\nu))$
- 20: $\tilde{\mathbf{x}} \leftarrow \mathbf{Q}(\mathbf{\Gamma} + \nu_* \mathbf{I})^{-1} \mathbf{Q}^H \mathbf{b}$
- 21: **return** $\tilde{\mathbf{x}} / \|\tilde{\mathbf{x}}\|_2$
- 22: **end function**

C. Phased-array optimization

In contrast to the previous section, the phased-array case does not admit a direct solution. Nevertheless, we will show that phased-array codebooks can be obtained via semidefinite programming (SDP) [23], as described in Algorithm 2.

Phased array codebooks \mathcal{C}_\circ and \mathcal{W}_\circ yield the following form of Problem (8):

$$\underset{\mathbf{x} \in \mathbb{C}^P}{\text{maximize}} \quad \Re(\mathbf{b}^H \mathbf{x}) \quad (13a)$$

$$\text{s.t.} \quad \mathbf{x}^H \mathbf{G} \mathbf{x} \leq \varepsilon, \quad (13b)$$

$$(\forall p \in [P]) \quad \mathbf{x}^H \mathbf{e}_p \mathbf{e}_p^T \mathbf{x} = 1/P, \quad (13c)$$

where $\mathbf{e}_p = [\mathbf{I}]_{:,p}$ is the p -th standard basis vector. We will now propose a method to solve (13) via SDP.

Proposition 3. *A solution to Problem (13) is given by*

$$\mathbf{x}_* = \tilde{\mathbf{x}} \frac{\tilde{\mathbf{x}}^H \mathbf{b}}{\|\tilde{\mathbf{x}}\|_2}, \quad \tilde{\mathbf{x}} = \sqrt{\sigma_{\max}(\tilde{\mathbf{X}})} \mathbf{v}_{\max}(\tilde{\mathbf{X}}),$$

where $\sigma_{\max}(\tilde{\mathbf{X}})$ and $\mathbf{v}_{\max}(\tilde{\mathbf{X}})$ are the largest eigenvalue and the corresponding eigenvector, respectively, of a solution $\tilde{\mathbf{X}}$ to the following nonconvex SDP problem:

$$\underset{\mathbf{X} \in \mathbb{S}^P}{\text{maximize}} \quad \langle \mathbf{b} \mathbf{b}^H, \mathbf{X} \rangle \quad (14a)$$

$$\text{s.t.} \quad \langle \mathbf{G}, \mathbf{X} \rangle \leq \varepsilon, \quad (14b)$$

$$(\forall p \in [P]) \quad \langle \mathbf{e}_p \mathbf{e}_p^H, \mathbf{X} \rangle = 1/P, \quad (14c)$$

$$\mathbf{X} \succcurlyeq \mathbf{0}, \quad (14d)$$

$$\text{rank}(\mathbf{X}) \leq 1. \quad (14e)$$

Algorithm 2 Phased CISSIR optimization.

Require: $\mathbf{F}(t), \mathbf{Y}, \mathbf{Z}, \varepsilon, \beta$

- 1: $\mathbf{G}_{\text{tx}}, \mathbf{G}_{\text{rx}} \leftarrow \text{INTEGRALSPLIT}(\mathbf{F}(t))$ ▷ Def. 1
- 2: $\mathbf{W} \leftarrow \text{SDPCODEBOOK}(\mathbf{Y}, \mathbf{G}_{\text{tx}}, \varepsilon^\beta)$
- 3: $\mathbf{C} \leftarrow \text{SDPCODEBOOK}(\mathbf{Z}, \mathbf{G}_{\text{rx}}, \varepsilon^{2-\beta})$
- 4: **return** \mathbf{W}, \mathbf{C}
- 5: **function** $\text{SDPCODEBOOK}(\mathbf{B}, \mathbf{G}, \varepsilon)$
- 6: **for** $r = 1, 2, \dots, R := \text{NUMCOLUMNS}(\mathbf{G})$ **do**
- 7: $\mathbf{b} \leftarrow [\mathbf{B}]_{:,r}$
- 8: $\tilde{\mathbf{X}} \leftarrow \text{SOLVESDP}(\mathbf{b}, \mathbf{G}, \varepsilon)$ ▷ (14a)–(14d)
- 9: $\tilde{\mathbf{x}} \leftarrow \sqrt{\sigma_{\max}(\tilde{\mathbf{X}})} \mathbf{v}_{\max}(\tilde{\mathbf{X}})$
- 10: $\mathbf{x}_r \leftarrow \tilde{\mathbf{x}}(\tilde{\mathbf{x}}^H \mathbf{b} / \|\tilde{\mathbf{x}}\|_2)$
- 11: **end for**
- 12: **return** $[\mathbf{x}_1, \mathbf{x}_2, \dots, \mathbf{x}_R]$
- 13: **end function**

Proof. We first note that any solution \mathbf{x}_* to (13) must fulfill $\Re(\mathbf{b}^H \mathbf{x}_*) = |\mathbf{b}^H \mathbf{x}_*|$. This follows from the fact that, for any feasible \mathbf{x}_f , we can construct another feasible $\tilde{\mathbf{x}}_f$ such that

$$\Re(\mathbf{b}^H \mathbf{x}_f) \leq |\mathbf{b}^H \mathbf{x}_f| = \Re(\mathbf{b}^H \tilde{\mathbf{x}}_f), \quad \tilde{\mathbf{x}}_f = \mathbf{x}_f (\mathbf{x}_f^H \mathbf{b} / |\mathbf{x}_f^H \mathbf{b}|).$$

Consequently, we can substitute the objective function in (13) with $|\mathbf{b}^H \mathbf{x}|^2 = \mathbf{x}^H \mathbf{b} \mathbf{b}^H \mathbf{x}$. In addition to this, we note the trace circular property ($\forall \mathbf{A} \in \mathbb{S}^M, \forall \mathbf{x} \in \mathbb{C}^M$):

$$\mathbf{x}^H \mathbf{A} \mathbf{x} = \text{tr}(\mathbf{x}^H \mathbf{A} \mathbf{x}) = \text{tr}(\mathbf{x} \mathbf{x}^H \mathbf{A}) = \langle \mathbf{A}, \mathbf{x} \mathbf{x}^H \rangle,$$

which allows us to express Problem (13) in terms of inner products as (14), such that $\tilde{\mathbf{X}} = \mathbf{x}_* \mathbf{x}_*^H$ and \mathbf{x}_* solves (13). \square

A convex relaxation of Problem (14) can be obtained by dropping the nonconvex constraint (14e). A solution $\tilde{\mathbf{X}}$ to the convex SDP problem (14a)–(14d) is not guaranteed to have rank one, but we can further elaborate on $\text{rank}(\tilde{\mathbf{X}})$ by relaxing constraint (14c):

$$\underset{\mathbf{X} \in \mathbb{S}^P}{\text{maximize}} \quad \langle \mathbf{b} \mathbf{b}^H, \mathbf{X} \rangle \quad (15a)$$

$$\text{s.t.} \quad \langle \mathbf{G}, \mathbf{X} \rangle \leq \varepsilon, \quad (15b)$$

$$(\forall p \in [P]) \quad \langle \mathbf{e}_p \mathbf{e}_p^H, \mathbf{X} \rangle \leq 1/P, \quad (15c)$$

$$\mathbf{X} \succcurlyeq \mathbf{0}. \quad (15d)$$

Problem (15) is also known as a *semidefinite packaging* problem, and Sagnol [25] proved that it always has a rank-one solution. Therefore, the solution $\tilde{\mathbf{X}}$ to (14a)–(14d) will also have rank one if it coincides with a solution to (15) for given \mathbf{b}, \mathbf{G} , and ε .

Furthermore, we know that $\exists \varepsilon_* \leq \mathbf{b}^H \mathbf{G} \mathbf{b}$ such that $\forall \varepsilon \geq \varepsilon_*$ $\text{rank}(\tilde{\mathbf{X}}) = 1$ (cf. Remark 2). Unfortunately, ε_* cannot be easily narrowed down further, but we can still assess the rank of $\tilde{\mathbf{X}}$ through the ratio between its spectral and nuclear norms:

$$\Upsilon(\tilde{\mathbf{X}}) := \frac{\|\tilde{\mathbf{X}}\|_2}{\|\tilde{\mathbf{X}}\|_*} = \frac{\sigma_{\max}(\tilde{\mathbf{X}})}{\text{tr}(\tilde{\mathbf{X}})} \in [1/P, 1], \quad (16)$$

for which we know that $\Upsilon(\tilde{\mathbf{X}}) = 1 \iff \text{rank}(\tilde{\mathbf{X}}) = 1$. In Section V, we use this fact to evaluate the feasibility of Algorithm 2 in our scenarios.

IV. PERFORMANCE BOUNDS AND PARAMETER SELECTION

The proposed Algorithms 1–2 in Section III aim to reduce the max. SI $\mathfrak{m}_{\mathbf{F}}(\mathbf{C}, \mathbf{W})$ in (5) according to the parameters ε and β . We analyze now the effect of SI before the ADCs for the hybrid-beamforming system in Section II-A, in order to provide recommendations for the choice of said parameters.

In Section IV-A, we derive a theoretical bound on the variance of the quantization noise introduced by the ADC, while we also comment on saturation. In Section IV-B, we extend the derived bound to the signal-to-noise ratio (SNR) for analog orthogonal frequency-division multiplexing (OFDM) radar, which is a relevant case for ISAC [1]–[5]. Finally, in Section IV-C we discuss how to select the target SI ε based on the derived bounds and our signal knowledge.

A. Self-interference impact at the analog-to-digital converter

ADCs have limited dynamic range, and this can be critical for ISAC in the face of SI. In particular, the ADC bit resolution Q causes signal quantization, which we have modeled as $u_k[i]$ in (4), following the well-established assumption of uniform white quantization noise [26]. That is, we assume $u_k[i]$ is independent of the ADC's input signal, with i.i.d. $\Re(u_k[i])$ and $\Im(u_k[i])$ drawn from $\mathcal{U}(-\frac{\Delta}{2}, \frac{\Delta}{2})$. The quantization step Δ can then be expressed in terms of the ADC's full-scale value r_{fs} and the bit resolution Q as $\Delta = 2r_{\text{fs}}/2^Q$, for which the quantization noise power equals

$$\sigma_Q^2 := \mathbb{E}[|u_k[i]|^2] = 2 \frac{\Delta^2}{12} = \frac{2r_{\text{fs}}^2}{3} 2^{-2Q}. \quad (17)$$

In order to minimize $\sigma_Q^2 \propto r_{\text{fs}}^2$, we can leverage signal knowledge for gain control, so that we set the smallest r_{fs} to avoid saturation. For example, we can set

$$r_{\text{fs}} = \gamma \max_{\substack{t \in [0, T+T_c] \\ k \in [K]}} \left| \sum_{\ell=1}^L \left((\mathbf{c}_{i(k)}^H \mathbf{F} \mathbf{w}_{j(\ell)}) * s_{\ell} \right) (t) \right|, \quad (18)$$

where we assume knowledge of the SI channel $\mathbf{F}(t)$ and the TX signals $s(t)$ during transmission, and we choose a back-off term $\gamma > 1$ to account for the unknown radar channel $\mathbf{H}_r(t)$. The condition to avoid saturation is

$$\gamma \geq \frac{\max_{t,k} \left| \sum_{\ell=1}^L \left((\mathbf{c}_{i(k)}^H (\mathbf{H}_r + \mathbf{F}) \mathbf{w}_{j(\ell)}) * s_{\ell} \right) (t) \right|}{\max_{t,k} \left| \sum_{\ell=1}^L \left((\mathbf{c}_{i(k)}^H \mathbf{F} \mathbf{w}_{j(\ell)}) * s_{\ell} \right) (t) \right|}.$$

Therefore, we can set γ fairly close to 1 in practice, since the contribution from the SI channel $\mathbf{F}(t)$ is typically orders of magnitude larger than the backscattered power over $\mathbf{H}_r(t)$.

We will now show how the sampling scheme in (17)–(18) yields an upper bound on the ADC noise as a function of the max. SI. The derived bound only depends on generic TX-signal properties, namely the TX power P_{tx} and the peak-to-average power ratio (PAPR) of each signal, ($\forall \ell \in [L]$) $\rho_{s_{\ell}}$:

$$P_{\text{tx}} := \sum_{\ell=1}^L \frac{1}{T} \int_0^T |s_{\ell}(t)|^2 dt = \frac{1}{T} \sum_{\ell=1}^L |s_{\ell}|_2^2, \quad (19)$$

$$\rho_{s_{\ell}} := T |s_{\ell}|_{\infty}^2 / |s_{\ell}|_2^2. \quad (20)$$

Lemma 1. Consider the system model in Section II, with the max. SI $\mathfrak{m}_{\mathbf{F}}(\mathbf{C}, \mathbf{W})$ in (5), the RX signal $\mathbf{r}(t)$ in (3), sampled at $1/T_S$ to obtain $\hat{\mathbf{r}}[i]$ in (4). Assuming white quantization noise, RX gain control as per (17)–(18), and the TX-signal properties in (19)–(20), then we have:

$$\mathbb{E} \left[\|\hat{\mathbf{r}}[i] - \mathbf{r}(iT_S)\|_2^2 \right] = \sum_{k=1}^K (\sigma_{\text{T}}^2 + \sigma_Q^2) \leq K \sigma_{\text{T}}^2 + K \frac{2\gamma^2 P_{\text{tx}}}{3} 2^{-2Q} \mathfrak{m}_{\mathbf{F}}^2(\mathbf{C}, \mathbf{W}) \sum_{\ell=1}^L \rho_{s_{\ell}}. \quad (21)$$

Proof. The proof is given in Appendix C. \square

Corollary 1. Let us assume the same system model as for Lemma 1, but with the channel propagation represented by discrete convolution with $\bar{\mathbf{H}}[i] = \bar{\mathbf{H}}_r[i] + \bar{\mathbf{F}}[i]$, i.e., ($\forall k \in [K]$):

$$\bar{r}_k[i] = \sum_{\ell=1}^L \left((\mathbf{c}_k^H \bar{\mathbf{H}} \mathbf{w}_{\ell}) * \bar{s}_{\ell} \right) [i], \quad (\forall \ell \in [L]) \quad \bar{s}_{\ell}[i] := s_{\ell}(iT_S).$$

Then, (21) still holds with $J = \lfloor (T + T_c)/T_S \rfloor$ and $\mathfrak{m}_{\bar{\mathbf{F}}}(\mathbf{C}, \mathbf{W}) = \max_{k,\ell} \sum_{i=1}^J |\mathbf{c}_k^H \bar{\mathbf{F}}[i] \mathbf{w}_{\ell}|$.

Proof. The proof follows from the fact that Young's inequality in Lemma 1's proof also applies to the discrete convolution [27, Theorem (20.18)]. \square

Lemma 1 allows us to assess the quantization noise induced by multipath SI for given beamforming codebooks, which we validate in Section V via simulations, thanks to Corollary 1. Lemma 1 also provides us with a rule to select the target SI ε in Problems 7–8, as we discuss in Section IV-C.

The target SI ε does not explicitly consider the saturation effect due to SI, which can occur at any point of the signal path, especially at the RX antennas or the low-noise amplifier (LNA). Nevertheless, the parameter β in (9) allows us to distribute SI-reduction flexibly between TX and RX beamforming to avoid saturation. In other words, we can set β such that $\varepsilon^{\beta} \geq \max_{\ell \in [L]} \mathbf{w}_{\ell}^H \mathbf{G}_{\text{tx}} \mathbf{w}_{\ell}$ satisfies any relevant saturation criteria.

B. Signal-to-noise ratio for analog OFDM radar

Lemma 1 provides a bound on noise variance as a function of the max. SI $\mathfrak{m}_{\mathbf{F}}(\mathbf{C}, \mathbf{W})$. Based on this bound, we focus now on analog beamforming and OFDM radar to extend our performance analysis to the sensing SNR, which is the main performance indicator for sensing detection and estimation [7].

Under analog beamforming, we have $K = L = 1$ RF chains. As a result, we only transmit a signal $\mathbf{s}(t) = s(t) \in \mathbb{C}$, and we receive $\mathbf{r}(t) = r(t) \in \mathbb{C}$ as:

$$r(t) = \left(\underbrace{(\mathbf{c}_o^H \mathbf{F} \mathbf{w}_o)}_{=: h_{\text{si}}} + \underbrace{(\mathbf{c}_o^H \mathbf{H}_r \mathbf{w}_o)}_{=: h_{\text{r}}} * s \right) (t), \quad (22)$$

where $\mathbf{c}_o \in \mathbb{C}^M$ and $\mathbf{w}_o \in \mathbb{C}^N$ form our selected TX-RX beamforming pair. This beamforming pair yields the single-antenna equivalent channels $h_{\text{si}}(t)$ and $h_{\text{r}}(t)$, which we assume passband filtered according to the signal bandwidth B .

Furthermore, if we employ OFDM waveforms, we can assume our TX signal to be stationary with almost flat power

spectral density $S(f)$ [5], [7]. In other words, ($\forall f \in [f_c - B/2, f_c + B/2]$) $S(f) \approx P_{\text{tx}}/B$, and hence:

$$\mathbb{E}[|r(t)|^2] = \zeta \frac{P_{\text{tx}}}{B} |h_{\text{r}}|_2^2 \approx \int_{f_c - B/2}^{f_c + B/2} \frac{P_{\text{tx}}}{B} |H_{\text{r}}(f)|^2 df, \quad (23)$$

with $\zeta \approx 1$. Assuming favorable Nyquist conditions so that $\mathbb{E}[|\hat{r}[i]|^2] = \mathbb{E}[|r(t)|^2]$, we can combine (23) with Lemma 1 to bound the SNR of the RX sensing signal $\hat{r}[i]$ in (4) as:

$$\text{SNR} = \frac{\mathbb{E}[|r(t)|^2]}{\sigma_{\text{T}}^2 + \sigma_{\text{Q}}^2} \geq \frac{\zeta |h_{\text{r}}|_2^2 P_{\text{tx}}/B}{\sigma_{\text{T}}^2 + \frac{2}{3} 2^{-2Q} \gamma^2 \mathbf{m}_{\text{F}}^2(\mathbf{C}, \mathbf{W}) P_{\text{tx}} \rho_{\text{s}}}. \quad (24)$$

The bound in (24) allows us to evaluate sensing performance theoretically with respect to the max. SI $\mathbf{m}_{\text{F}}(\mathbf{C}, \mathbf{W})$ and the target SI ε . Nevertheless, choosing ε from (24) is challenging in practice, as we often lack the following information:

- 1) The radar channel $\mathbf{H}_{\text{r}}(t)$, and thus $h_{\text{r}}(t)$. Even if we know $\mathbf{H}_{\text{r}}(t)$, we cannot compute $|h_{\text{r}}|_2$ before optimizing $(\mathbf{c}_{\circ}, \mathbf{w}_{\circ})$. However, we can approximate it from the reference beamforming pair $(\mathbf{z}_{\circ}, \mathbf{y}_{\circ})$ as $|h_{\text{r}}|_2 \approx |\mathbf{z}_{\circ} \mathbf{H}_{\text{r}} \mathbf{y}_{\circ}|_2$, if the codebook deviations σ_{tx}^2 and σ_{rx}^2 in (6) are low enough.
- 2) The PAPR ρ_{s} , since the signal $s(t)$ may also be unknown during optimization.

To address this issue, we suggest a more practical approach in Section IV-C.

C. Selection of the target self-interference

To set the target SI ε in Algorithms 1–2, we first suggest fixing a target quantization noise σ_{\star}^2 , either from (24) if $|h_{\text{r}}|_2^2$ is known, or with respect to the thermal noise σ_{T}^2 otherwise. From Lemma 1, we select the target SI as

$$\varepsilon = \sqrt{\frac{3\sigma_{\star}^2 2^{2Q}}{2\gamma^2 P_{\text{tx}} \bar{\rho}_{\text{s}}}}, \quad (25)$$

which guarantees $\sigma_{\text{Q}}^2 \leq \sigma_{\star}^2$. The estimated PAPR $\bar{\rho}_{\text{s}} > 0$ is computed from the available information on $s(t)$ during optimization. Some options to compute $\bar{\rho}_{\text{s}}$ include:

1) *Matched optimization*: In the best-case scenario, we do know $s(t)$ and we can just choose $\bar{\rho}_{\text{s}} = \sum_{\ell=1}^L \rho_{s_{\ell}}$ in (25). This can be the case if the optimization algorithm is fast enough to be run for every new TX symbol, e.g., if it has a semi-closed form as in Section III-B.

2) *Average optimization*: In certain setups, it might suffice to ensure that the quantization noise variance is below σ_{\star}^2 only for the average TX symbol. In this case, the codebooks can be optimized a priori with $\bar{\rho}_{\text{s}} = \sum_{\ell=1}^L \mathbb{E}[\rho_{s_{\ell}}]$.

3) *Quantile optimization*: If a certain noise level must be guaranteed, yet memory and speed limitations rule out the previous methods, then we can make $\bar{\rho}_{\text{s}} = \sum_{\ell=1}^L \mathbb{E}[\rho_{s_{\ell}}]/\alpha$. This PAPR estimate controls the probability of a TX symbol to exceed the noise threshold via Markov's inequality, i.e.:

$$\Pr(\sigma_{\text{Q}}^2 \geq \sigma_{\star}^2) \leq \alpha.$$

V. NUMERICAL RESULTS

After our theoretical analysis, now we evaluate CISSIR with a series of simulation experiments. First, we present some sensing results in Section V-A, which validate the performance bounds derived in Section IV. Afterwards, we study the impact of SI reduction on communication, in Section V-B. We continue with an investigation of the communication-sensing trade-off in Section V-C, both for CISSIR and for the baseline LoneSTAR [14]. Finally, we complete our numerical evaluation with a discussion on the time complexity and feasibility of the studied algorithms.

Our simulation environment has been developed from previous work in [29] and is based on SionnaTM, a Python library by Nvidia that integrates link-level and ray-tracing simulation tools [24]. Our reference standard is 5G NR frequency range 2 (FR2). As such, we employ OFDM waveforms in the millimeter wave (mmWave) frequency with quadrature amplitude

TABLE I
SIMULATION PARAMETERS

NAME	VALUE	SYMBOL
A. Signal parameters		
Carrier frequency	28 GHz	f_c
Wavelength	10.7 mm	λ
Waveform	(cyclic-prefix) OFDM	
5G NR numerology	3 [19]	μ
Subcarrier spacing	120 kHz	SCS
Symbol duration	9.44 μ s	T
Max. channel delay	1.11 μ s	T_c
B. Antenna parameters		
TX antenna elements	8	N
RX antenna elements	8	M
TX codebook size	27	L'
RX codebook size	27	K'
TX RF chains	1	L
RX RF chains	1	K
Ant. element spacing	5.35 mm	$\lambda/2$
Ant. element pattern	TR 38.901 [28]	
Elevation angle	0 $^{\circ}$	
Sector coverage	120 $^{\circ}$	
C. SI parameters		
Min. TX- RX separation	5.35 mm	$\lambda/2$
Wall distance	4 m	
Wall azimuth	65 $^{\circ}$	
Multipath max. SI	-54.5 dB	$\mathbf{m}_{\text{F}}(\mathbf{Z}, \mathbf{Y})$
Single-path max. SI	-60.6 dB	$\mathbf{m}_{\text{F}_1}(\mathbf{Z}, \mathbf{Y})$
D. Sensing parameters		
TX power	30 dBm	P_{tx}
Sampling interval	0.51 ns	T_{S}
Number of symbols	1000	
Number of subcarriers	1680	
Bandwidth	200 MHz	B
Modulation	64 QAM	
Target azimuth	-39 $^{\circ}$	
Target distance	40 m	
Target RCS	1 m ²	
Target RX power	-81.0 dBm	
Thermal noise	-90.8 dBm	σ_{T}^2
ADC bits	6 bit	Q
E. Communication parameters		
UE antennas	1	
Number of subcarriers	420	
Number of symbols	14 (2 pilots)	
Bandwidth	50 MHz	
Modulation	4 QAM	
Code rate	0.7	
Bitrate	62.3 Mbit/s	
Channel model	LoS outdoor UMi [28]	

modulation (QAM), and subcarrier spacing (SCS) according to a given numerology μ [19]. Likewise, our reference beam codebooks \mathbf{Y} and \mathbf{Z} are given by the columns of a discrete Fourier transform (DFT) matrix with an oversampling factor $O_1 = 4$. We assume uniform linear arrays (ULAs) with $M = N = 8$ antennas, radiation pattern according to TR 38.901 [28], fixed elevation, and $L' = K' = 27$ beams, corresponding to a full grid over a sector coverage of 120° . Table I contains the complete parameter list.

We simulate the SI channel via ray-tracing, with $D = 2$ paths corresponding to $\mathbf{F}_1(t)$ and $\mathbf{F}_2(t)$ (see Figs. 1–2). The component $\mathbf{F}_1(t)$ is produced by a spherical wave model, similar to the flat MIMO SI channel in [14]–[16], while we add the clutter $\mathbf{F}_2(t)$ as a wall-reflected path. Leveraging Corollary 1, we approximate the continuous channels by their discrete versions sampled at $T_S \ll 1/B$, and we apply a passband filter to account for the sensing bandwidth B .

We optimize the codebooks via Algorithms 1–2 for tapered beamforming and phased arrays, respectively, with $\beta = 1$ (and thus $\epsilon = \varepsilon$) to give equal importance to TX and RX codebook deviation. In Sections V-A–V-B, we use phased arrays as obtained by Algorithm 2, for which we use CVXPY to solve the convex SDP problem (14a)–(14d) therein [30].

A. Sensing performance

Our primary goal, as detailed in Sections II–III, is to design ISAC beam codebooks for which the SI-induced quantization noise is reduced. To this aim, we have derived the performance bound (24) for the sensing SNR in Section IV, which we now compare with our experimental results.

For this, we have simulated a sensing channel $\mathbf{H}(t) = \mathbf{F}(t) + \mathbf{H}_r(t)$ in a single-target scenario. The sensing channel is displayed in Fig. 2, beamformed with a reference beam pair $(\mathbf{z}_o, \mathbf{y}_o)$ pointing towards the target. We optimize $(\mathbf{c}_o, \mathbf{w}_o)$ with respect to this beam pair for different values of the target SI ε . For each optimized $(\mathbf{c}_o, \mathbf{w}_o)$, we simulate the signals $s(t)$

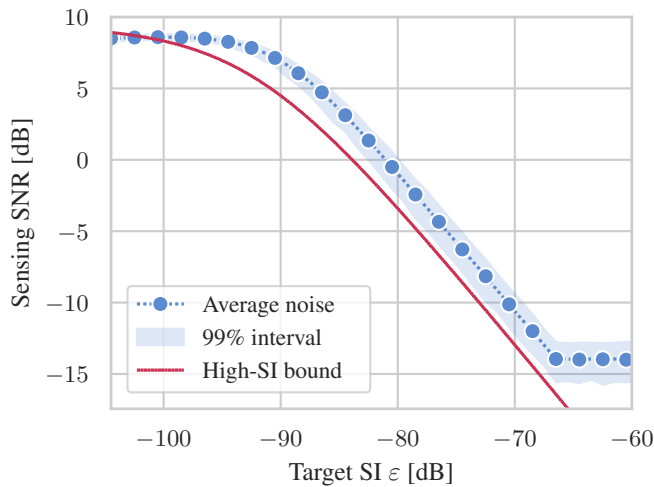


Fig. 3. Simulated sensing SNR (symbol-averaged noise and 99% interval) and approximate bound for high SI, in function of the target SI ε .

and $r(t)$ in (22) according to the parameters in Table I.D, and we estimate the sensing SNR of the digital RX signal $\hat{r}(t)$.

We show the resulting SNR in function of ε in Fig. 3. We also plot the theoretical bound (24), where we replace the max. SI $\mathbf{m}_F(\mathbf{C}, \mathbf{W})$ with ε , we set $|h_r|_2 = |\mathbf{z}_o^H \mathbf{H}_r \mathbf{y}_o|_2$, we compute the PAPR $\rho_s \approx 9.6$ dB as the average over symbols (cf. Section IV-C2), and we make $\gamma = 1$ and $\zeta \approx 0.98$. We remind the reader that this bound is an a priori approximation of (24) that is only valid for the average noise over TX symbols, and for high SI such that $|h_r|_2 = |\mathbf{c}_o^H \mathbf{H}_r \mathbf{w}_o|_2 \approx |\mathbf{z}_o^H \mathbf{H}_r \mathbf{y}_o|_2$.

In Fig. 3, the SI constraint (8b) only becomes active for $\mathbf{c}_o, \mathbf{w}_o$ when the target SI ε is below -68 dB. In that regime, we observe a gap of at most 2.5 dB between the sensing SNR, when the noise is symbol-averaged, and the bound in (24). This bound gap, which is due to Young's inequality (cf. Appendix C), compensates to some extent the SNR fluctuation caused by the PAPR variation over symbols. As expected, this theoretical bound becomes invalid for very low SI, due to a gain loss induced by high codebook deviations $\sigma_{\text{tx}}^2 = \|\mathbf{W} - \mathbf{Y}\|_F^2$ and $\sigma_{\text{rx}}^2 = \|\mathbf{C} - \mathbf{Z}\|_F^2$.

To illustrate codebook deviation, we compare some reference TX beams from \mathbf{Y} with those from \mathbf{W} in Fig. 4. Here, we have chosen very low ε , which leads to higher secondary lobes and gain loss in the main lobe, in the best case. In the worst case, beam misalignment occurs, as can be seen near the sector edges in our simulation. As a result, the angular coverage of CISSIR deteriorates as we decrease the max. SI.

Motivated by this effect, we investigate next the impact of SI reduction and codebook deviation on communication.

B. Communication performance

We evaluate communication performance via link-level simulations from a base station (BS) towards a single-antenna

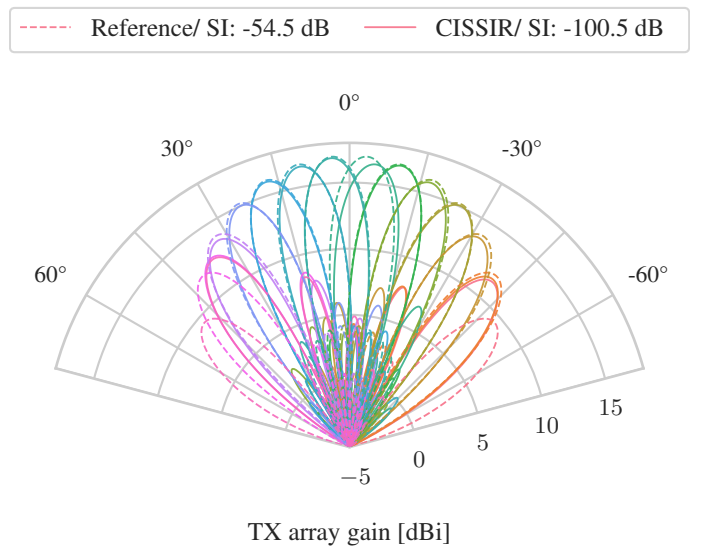


Fig. 4. Selected beams from the reference TX codebook \mathbf{Y} and from phased-array CISSIR \mathbf{W} , with noticeable beam misalignment near $\pm 60^\circ$.

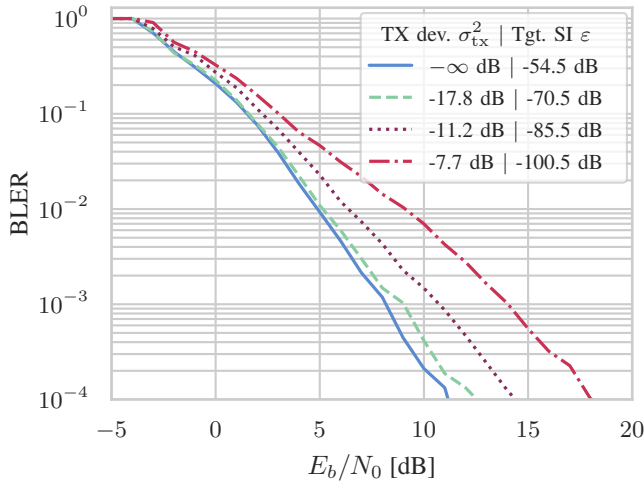


Fig. 5. BLER for different analog CISSIR codebooks. The solid line corresponds to the TX reference codebook.

user equipment (UE), placed randomly on an urban micro-cell (UMi) sector under line-of-sight (LoS) outdoor conditions [28]. The BS selects the strongest beam from its analog codebook for transmission, whereas the UE performs least-squares (LS) channel estimation from 2 OFDM pilot symbols, and linear-minimum-mean-square-error (LMMSE) equalization before decoding. The data in the remaining 12 TX symbols is low-density parity-check (LDPC)-encoded and constitutes a single block (see Table I.E for more details).

We simulate the block error rate (BLER) as a function of the energy per bit to noise power spectral density (E_b/N_0) for the 5G-NR TX reference codebook, as well as for three CISSIR TX codebooks with different levels of target SI ε and codebook deviation σ_{tx}^2 . The resulting BLER curves in Fig. 5 show a progressive degradation of the communication performance as

we reduce ε . Nevertheless, this degradation is not relevant for small values of σ_{tx}^2 , which allows us to add 16 dB of extra SI attenuation while losing at most 1 dB of TX power for communication. As we further decrease the target SI ε , however, the codebook deviation increases, and we must add up to 6 dB to the E_b/N_0 to maintain the reference BLER.

From these experiments, we conclude that extreme SI reduction degrades communication, as σ_{tx}^2 increases and gives rise to beam misalignment and poorer angular coverage.

C. Trade-off between self-interference and codebook deviation

From the analysis in Sections V-A–V-B, we consider max. SI and codebook deviations good indicators for sensing and communication performance, respectively. Thus, we use them now to study the sensing-communication trade-off of CISSIR and compare it to that of our baseline LoneSTAR [14].

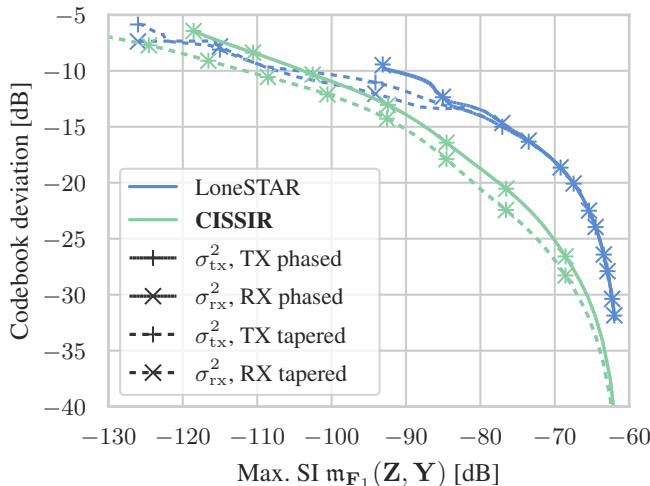
LoneSTAR codebook optimization, described in [14, Algorithm 1], assumes a frequency-flat MIMO SI channel that can be modeled as a single matrix $\bar{\mathbf{H}} \in \mathbb{C}^{M \times N}$. Given $\bar{\mathbf{H}}$, it minimizes the following SI quantity:

$$\|\mathbf{C}\bar{\mathbf{H}}\mathbf{W}\|_{\text{F}}^2, \quad (26)$$

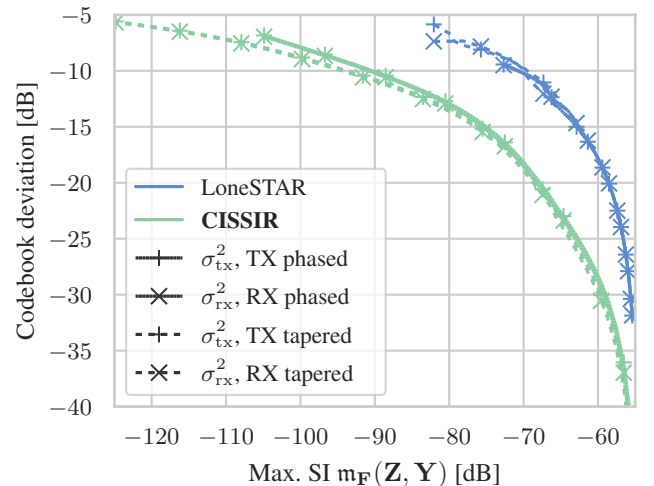
under per-antenna power constraints and a maximum codebook deviation $\sigma_{\text{cb}}^2 \geq \max\{\sigma_{\text{tx}}^2, \sigma_{\text{rx}}^2\}$, that is chosen heuristically. The authors follow an alternating approach so that the TX codebook \mathbf{W} is optimized first and then plugged in (26) for the optimization of the RX codebook \mathbf{C} . In addition to this, the codebooks are projected to their feasibility sets, $\mathcal{W} \ni \mathbf{W}$ and $\mathcal{C} \ni \mathbf{C}$, after the corresponding optimization step.

For a fair comparison between CISSIR and LoneSTAR, we first consider a simplified SI model that only includes the direct coupling $\mathbf{F}_1(t)$, and we set $\bar{\mathbf{H}} = \mathbf{F}_1(\tau_1)$ in (26) for LoneSTAR optimization, with τ_1 the mean path delay. For CISSIR, we simply set $\mathbf{F}(t) = \mathbf{F}_1(\tau_1)\delta(t - \tau_1)$ in Algorithms 1–2.

We optimize LoneSTAR and CISSIR for different values of σ_{cb}^2 and target SI ε , respectively, and plot the resulting trade-off curves in Fig. 6a, assuming either phased or tapered arrays.



(a) Single-path SI channel $\mathbf{F}_1(t)$.



(b) Multipath SI channel $\mathbf{F}(t)$.

Fig. 6. TX and RX codebook deviations σ_{tx}^2 and σ_{rx}^2 as functions of the max. SI for LoneSTAR and CISSIR, both for phased and tapered arrays.

TABLE II
ALGORITHMIC METRICS FOR LONESTAR (PHASED AND TAPERED) AND CISSIR

SI channel model	Optimization time (1st – 3rd quartiles)			Minimum feasible SI		Largest SI gap	
	LoneSTAR	Phased CISSIR	Tapered CISSIR	Phased CISSIR	Tapered CISSIR	Phased CISSIR	Tapered CISSIR
Single-path $\mathbf{F}_1(t)$	0.16 s–1.02 s	1.20 s–1.48 s	6.5 ms–7.7 ms	–123 dB	–165.4 dB	0.0 dB	0.5 dB
Multipath $\mathbf{F}(t)$	-	1.14 s–1.39 s	4.6 ms–8.2 ms	–108 dB	–132.1 dB	0.4 dB	1.9 dB

Here, we observe that CISSIR can reduce SI further than LoneSTAR for the same σ_{tx}^2 and σ_{rx}^2 , with a max. SI gap going up to 14 dB for a codebook deviation around -18 dB. For the same deviation, CISSIR reaches around 2 dB more SI-reduction for tapered ($\mathcal{W}_{\triangleright}, \mathcal{C}_{\triangleright}$) than for phased arrays ($\mathcal{W}_{\circ}, \mathcal{C}_{\circ}$), which is expected since $\mathcal{W}_{\circ} \subset \mathcal{W}_{\triangleright}$ and $\mathcal{C}_{\circ} \subset \mathcal{C}_{\triangleright}$. For LoneSTAR, tapering allows for more SI reduction, but it performs similarly to phased arrays for max. SI over -85 dB, perhaps due to the considered per-antenna power constraint [14]. CISSIR curves coincide for TX and RX, which is expected for $\beta = 1$. In fact, a different choice of β would merely alter the parameter $\epsilon \in \{\epsilon^{\beta}, \epsilon^{2-\beta}\}$ in Problem (8), which would merely shift the curves horizontally along the max. SI axis in Fig. 6a.

In Fig. 6b, we plot the trade-off curves again for our full multipath SI model $\mathbf{F}(t)$. Since LoneSTAR only considers flat-frequency SI, we retain the $\mathbf{F}_1(t)$ -optimized LoneSTAR codebooks above to evaluate their performance under multipath SI. Unsurprisingly, LoneSTAR experiences a performance degradation in this multipath scenario, as it is unable to attain a max. SI below -83 dB. On the other hand, CISSIR can still reduce the max. SI well below -100 dB and -120 dB for phased and tapered arrays, respectively.

Overall, CISSIR performs better than LoneSTAR for the considered metrics, even under frequency-flat SI. In addition to this, CISSIR can achieve considerable multipath SI reduction.

D. Algorithmic performance

We finalize our investigation with some empirical results on the time complexity and feasibility of CISSIR, which we summarize in Table II.

To analyze time complexity, we report the first and third quartiles of the optimization time of the studied algorithms. Here, we can see that phased CISSIR is slower than LoneSTAR, which can be explained by the space lifting of the SDP problem; e.g., Algorithm 2 must optimize $L' N \times N$ matrices to retrieve the $N \times L'$ -sized TX codebook. On the other hand, tapered CISSIR is almost 200 times faster than its phased counterpart and up to 130 times faster than LoneSTAR, thanks to the semi-closed-form solution of Algorithm 1.

Regarding problem feasibility, we can compute the minimum feasible SI exactly for tapered CISSIR as $\min_{k,\ell} (\bar{\sigma}(\mathbf{z}_k, \mathbf{G}_{\text{rx}}) \bar{\sigma}(\mathbf{y}_{\ell}, \mathbf{G}_{\text{tx}}))$ (cf. Proposition 2). For phased arrays, we estimate the minimum feasible SI as the target SI ϵ for which $\Upsilon(\tilde{\mathbf{X}})$ in (16) is above 0.995 on average. In any case, we conclude that CISSIR provides optimal solutions in our scenarios for a wide range of ϵ , over 50 dB below the reference max. SI in Table I.

To conclude our discussion, we note that the original SI constraint (7b) is fulfilled quite tightly in our simulations. In fact, the “SI gap” between max. SI $\mathbf{m}_{\mathbf{F}}(\mathbf{C}, \mathbf{W})$ and target

SI ϵ is at most 0.4 dB for max. SI above -108 dB in our experiments, and it only increases to 2 dB for tapered CISSIR when it approaches its feasible SI. From this result, we can argue in favor of CISSIR as a good approximation to the original Problem (7), given the tightness of the restriction (11) in Proposition 1.

VI. CONCLUSION

In this paper, we have proposed codebooks with integral split for self-interference reduction (CISSIR) as an evolution of the existing beam codebooks in current mobile networks, both for hybrid and analog schemes. CISSIR achieves notable self-interference (SI) reduction and thus paves the way to integrated sensing and communication (ISAC) beyond 5G.

The proposed methodology allows a systematic optimization of phased-array and tapered beam codebooks via semidefinite programming and spectral decomposition, respectively. Our framework also provides performance guarantees regarding SI impairments in the analog domain. More specifically, we have derived an analytical bound on the quantization noise at the analog-to-digital converter, and we have proved its practicality via sensing simulations. Moreover, our link-level results show how CISSIR can reduce SI with a small impact on 5G-NR-based communication. Contrary to other available SI-reduced beam codebooks, our proposed method has easily interpretable optimization parameters, and it outperforms said codebooks for relevant ISAC performance indicators.

Future research can introduce other practical aspects into our optimization framework, including hybrid multiuser MIMO, calibration errors relative to the SI channel, or quantized beamforming.

APPENDIX

A. Proof of Proposition 1 (split of the original problem)

The rightmost inequality of (11) in Proposition 1.i follows by construction from (8)–(10):

$$\mathfrak{s}_{\mathbf{F}}(\mathbf{C}, \mathbf{W}) \leq \max_{k \in K'} \epsilon^{\beta/2} \max_{\ell \in L'} \epsilon^{(2-\beta)/2} = \epsilon.$$

Thus, it only remains to prove $\mathbf{m}_{\mathbf{F}}(\mathbf{C}, \mathbf{W}) \leq \mathfrak{s}_{\mathbf{F}}(\mathbf{C}, \mathbf{W})$ in Proposition 1.i. Using the SVD in Definition 1 and the

Cauchy-Schwarz inequality, we bound the argument inside $\mathbf{m}_F(\mathbf{C}, \mathbf{W}) := \max_{k \in [K'], \ell \in [L']} \int_0^{T_c} |\mathbf{c}_k^H \mathbf{F}(t) \mathbf{w}_\ell| dt$ as:

$$\begin{aligned} \int_0^{T_c} |\mathbf{c}_k^H \mathbf{F}(t) \mathbf{w}_\ell| dt &= \int_0^{T_c} |\mathbf{c}_k^H \mathbf{U}_t \Sigma_t^{1/2} \Sigma_t^{1/2} \mathbf{V}_t^H \mathbf{w}_\ell| dt \\ &\leq \int_0^{T_c} \left\| \Sigma_t^{1/2} \mathbf{U}_t^H \mathbf{c}_k \right\|_2 \left\| \Sigma_t^{1/2} \mathbf{V}_t^H \mathbf{w}_\ell \right\|_2 dt, \\ &\leq \sqrt{\int_0^{T_c} \left\| \Sigma_t^{1/2} \mathbf{U}_t^H \mathbf{c}_k \right\|_2^2 dt} \sqrt{\int_0^{T_c} \left\| \Sigma_t^{1/2} \mathbf{V}_t^H \mathbf{w}_\ell \right\|_2^2 dt} \\ &= \sqrt{\int_0^{T_c} \mathbf{c}_k^H \mathbf{U}_t \Sigma_t \mathbf{U}_t^H \mathbf{c}_k dt} \sqrt{\int_0^{T_c} \mathbf{w}_\ell^H \mathbf{V}_t \Sigma_t \mathbf{V}_t^H \mathbf{w}_\ell dt}. \quad (27) \end{aligned}$$

The desired inequality is obtained by applying max over $k \in [K']$ and $\ell \in [L']$ in (27).

For Proposition 1.ii, we note that any upper bound on $\mathfrak{s}_F(\mathbf{C}, \mathbf{W})$ can be separated into a single constraint for each of the $K' + L'$ codebook columns, as given by (8b). The objective function (7a) is also column-separable as a sum of terms of the form $(\forall k \in [K'], \forall \ell \in [L'])$:

$$\begin{aligned} \|\mathbf{c}_k - \mathbf{z}_k\|_2^2 &= (\mathbf{c}_k - \mathbf{z}_k)^H (\mathbf{c}_k - \mathbf{z}_k) \\ &= \|\mathbf{c}_k\|_2^2 + \|\mathbf{z}_k\|_2^2 - 2\Re(\mathbf{z}_k^H \mathbf{c}_k) = 2(1 - \Re(\mathbf{z}_k^H \mathbf{c}_k)), \\ \|\mathbf{w}_\ell - \mathbf{y}_\ell\|_2^2 &= 2(1 - \Re(\mathbf{y}_\ell^H \mathbf{w}_\ell)). \end{aligned}$$

From this reformulation of (7a), it is clear that minimizing the squared difference between codebook columns is equivalent to maximizing their inner product. Therefore, the restriction of Problem (7) in Proposition 1 is equivalent to the column-wise solutions to (8)–(9), as stated in Proposition 1.ii.

B. Proof of Proposition 2 (tapered beamforming solution)

The semi-closed form solution of Problem (12) in Proposition 2, \mathbf{x}_* , is obtained from the Lagrangian of (12):

$$\mathcal{L}(\mathbf{x}, \mu, \lambda) = -\Re(\mathbf{b}^H \mathbf{x}) + \mu (\mathbf{x}^H \mathbf{G} \mathbf{x} - \epsilon) + \lambda (\mathbf{x}^H \mathbf{x} - 1),$$

with $\mu \geq 0$. We notice that a convex relaxation of (12) can be simply obtained by replacing constraint (12c), $\mathbf{x}^H \mathbf{x} = 1$, with

$$\mathbf{x}^H \mathbf{x} \leq 1, \quad (12d)$$

and the Lagrangian would remain the same with the additional constraint $\lambda \geq 0$. We focus on this convex relaxation for the nontrivial case $\mathbf{b}^H \mathbf{G} \mathbf{b} > \epsilon$, and assume $\mu, \lambda > 0$, which requires the constraints (12b) and (12d) to be active.

Now, we look for the values of \mathbf{x}, μ, λ which make $\nabla \mathcal{L}(\mathbf{x}, \mu, \lambda) = 0$. Let us first evaluate the partial derivative with respect to \mathbf{x} to find a candidate solution \mathbf{x}_* :

$$\begin{aligned} \frac{\partial \mathcal{L}(\mathbf{x}_*, \mu, \lambda)}{\partial \mathbf{x}} &= -\mathbf{b} + 2\mu \mathbf{G} \mathbf{x}_* + 2\lambda \mathbf{x}_* = 0 \Rightarrow \\ \mathbf{x}_* &= \frac{1}{2} (\mu \mathbf{G} + \lambda \mathbf{I})^{-1} \mathbf{b} = \eta (\mathbf{Q} \mathbf{\Gamma} \mathbf{Q}^H + \nu \mathbf{I})^{-1} \mathbf{b} \\ &= \eta \mathbf{Q} \underbrace{(\mathbf{\Gamma} + \nu \mathbf{I})^{-1}}_{\mathbf{D}_\nu} \mathbf{Q}^H \mathbf{b}, \end{aligned}$$

where we have applied the eigendecomposition of $\mathbf{G} = \mathbf{Q} \mathbf{\Gamma} \mathbf{Q}^H$ and the variable changes $\eta = 1/2\mu$ and $\nu = \lambda/\mu$

for $\mu, \lambda, \eta, \nu > 0$. Notice that \mathbf{x}_* is obtained by multiplying \mathbf{b} with the PSD matrix $\mathbf{Q} \mathbf{D}_\nu \mathbf{Q}^H$, and scaling by η to ensure $\|\mathbf{x}_*\|_2 = 1$.

Due to complementary slackness, (12b) and (12d) must be tight for \mathbf{x}_* , i.e.:

$$\begin{aligned} \mathbf{x}_*^H \mathbf{x}_* &= \eta \mathbf{b}^H \mathbf{Q} \mathbf{D}_\nu \mathbf{Q}^H \mathbf{Q} \mathbf{D}_\nu \mathbf{Q}^H \mathbf{b} \eta = \eta^2 \mathbf{b}^H \mathbf{Q} \mathbf{D}_\nu^2 \mathbf{Q}^H \mathbf{b} = 1, \\ \mathbf{x}_*^H \mathbf{G} \mathbf{x}_* &= \eta \mathbf{b}^H \mathbf{Q} \mathbf{D}_\nu \mathbf{Q}^H \mathbf{Q} \mathbf{\Gamma} \mathbf{Q}^H \mathbf{Q} \mathbf{D}_\nu \mathbf{Q}^H \mathbf{b} \eta \\ &= \eta^2 \mathbf{b}^H \mathbf{Q} \mathbf{D}_\nu \mathbf{\Gamma} \mathbf{D}_\nu \mathbf{Q}^H \mathbf{b} = \epsilon. \end{aligned}$$

If we divide both expressions above by $\eta^2 > 0$, we obtain:

$$\begin{aligned} \mathbf{b}^H \mathbf{Q} \mathbf{D}_\nu \mathbf{\Gamma} \mathbf{D}_\nu \mathbf{Q}^H \mathbf{b} &= \frac{\epsilon}{\eta^2} = \epsilon \mathbf{b}^H \mathbf{Q} \mathbf{D}_\nu^2 \mathbf{Q}^H \mathbf{b} \\ \sum_{p=1}^P \frac{\sigma_p |\mathbf{q}_p^H \mathbf{b}|^2}{(\sigma_p + \nu)^2} &= \epsilon \sum_{p=1}^P \frac{|\mathbf{q}_p^H \mathbf{b}|^2}{(\sigma_p + \nu)^2}, \quad (28) \end{aligned}$$

where we have used the diagonality of \mathbf{D}_ν and $\mathbf{\Gamma}$ to write out the matrix multiplications. Since we are interested in $\nu > 0$, we can multiply both sides of (28) by the positive factor $\prod_{p=1}^P (\sigma_p + \nu)^2$ and rearrange to obtain $\mathcal{P}(\nu) = 0$, deriving the semi-closed form of \mathbf{x}_* .

The existence of \mathbf{x}_* is subject to the tightness of the convex relaxation of (12), and thus to the existence of a real positive root for $\mathcal{P}(\nu)$ in Proposition 2. For this, we have the sufficient but not necessary condition that the nonzero coefficients with the highest and lowest degree have opposite signs, which can be derived from Descartes' rule of signs [31]. For $\epsilon < \mathbf{b}^H \mathbf{G} \mathbf{b}$, the highest-degree coefficient c_{2P-2} is positive:

$$\begin{aligned} c_{2P-2} &= \sum_{p=1}^P (\sigma_p - \epsilon) |\mathbf{q}_p^H \mathbf{b}|^2 \\ &= \mathbf{b}^H \sum_{p=1}^P \sigma_p \mathbf{q}_p \mathbf{q}_p^H \mathbf{b} - \epsilon \mathbf{b}^H \mathbf{Q} \mathbf{Q}^H \mathbf{b} \\ &= \mathbf{b}^H \mathbf{G} \mathbf{b} - \epsilon \mathbf{b}^H \mathbf{b} = \mathbf{b}^H \mathbf{G} \mathbf{b} - \epsilon > 0. \end{aligned}$$

For the lowest-degree coefficient, we need to consider the rank of \mathbf{G} . If \mathbf{G} is not full rank, i.e., $R = P - \text{rank}(\mathbf{G}) > 0$, it can be proven by mathematical evaluation that the lowest nonzero coefficient has degree $2R - 2$ and equals:

$$c_{2R-2} = - \sum_{p: \sigma_p=0} \epsilon |\mathbf{q}_p^H \mathbf{b}|^2 \prod_{\sigma_q \neq 0} \sigma_q^2 < 0.$$

Therefore, $\mathcal{P}(\nu)$ always has a positive root for $\text{rank}(\mathbf{G}) < P$ and $\epsilon \in (0, \mathbf{b}^H \mathbf{G} \mathbf{b})$, as given by condition i in Proposition 2.

If \mathbf{G} is full rank (condition ii, the tightness of the convex relaxation is guaranteed by $\epsilon < \mathbf{b}^H \mathbf{G} \mathbf{b}$ and

$$\begin{aligned} c_0 &= \sum_{p=1}^P (\sigma_p - \epsilon) |\mathbf{q}_p^H \mathbf{b}|^2 \prod_{q \neq p} \sigma_q^2 < 0 \\ &= \sum_{p=1}^P \frac{(\sigma_p - \epsilon) |\mathbf{q}_p^H \mathbf{b}|^2}{\sigma_p^2} < 0 \\ \bar{\sigma}(\mathbf{b}, \mathbf{G}) &= \frac{\sum_{p=1}^P \sigma_p |\mathbf{q}_p^H \mathbf{b}|^2 / \sigma_p^2}{\sum_{p=1}^P |\mathbf{q}_p^H \mathbf{b}|^2 / \sigma_p^2} < \epsilon. \end{aligned}$$

We note that $\bar{\sigma}(\mathbf{b}, \mathbf{G})$ is a weighted average of $\{\sigma_p\}_{p=1}^P$.

C. Proof of Lemma 1 (quantization noise bound)

The total noise variance for $\hat{\mathbf{r}}[i]$ in (21) can be rewritten as

$$\begin{aligned} \mathbb{E} \left[\|\hat{\mathbf{r}}[i] - \mathbf{r}(iT_S)\|_2^2 \right] &= \mathbb{E} \left[\sum_{k=1}^K |\hat{r}_k[i] - r_k(iT_S)|^2 \right] \\ &= \sum_{k=1}^K \mathbb{E}[|v_k[i] + u_k[i]|^2] = \sum_{k=1}^K \mathbb{E}[|v_k[i]|^2] + \mathbb{E}[|u_k[i]|^2] \\ &= \sum_{k=1}^K (\sigma_T^2 + \sigma_Q^2) = K\sigma_T^2 + \frac{2Kr_{\text{fs}}^2}{3}2^{-2Q}, \quad (29) \end{aligned}$$

where we have used the definition of σ_Q^2 in (17). Now, we will turn our attention to r_{fs} in (18). Firstly, we note that

$$\begin{aligned} r_{\text{fs}} &= \gamma \max_{k \in [K]} \left| \sum_{\ell=1}^L (\mathbf{c}_{i(k)}^H \mathbf{F} \mathbf{w}_{j(\ell)}) * s_{\ell} \right|_{\infty} \\ &\leq \gamma \max_{k \in [K']} \left| \sum_{\ell=1}^L (\mathbf{c}_k^H \mathbf{F} \mathbf{w}_{j(\ell)}) * s_{\ell} \right|_{\infty}. \quad (30) \end{aligned}$$

For an arbitrary $k \in [K']$, we have:

$$\begin{aligned} \left| \sum_{\ell=1}^L (\mathbf{c}_k^H \mathbf{F} \mathbf{w}_{j(\ell)}) * s_{\ell} \right|_{\infty} &\stackrel{\text{a)}}{\leq} \sum_{\ell=1}^L |(\mathbf{c}_k^H \mathbf{F} \mathbf{w}_{j(\ell)}) * s_{\ell}|_{\infty} \stackrel{\text{b)}}{\leq} \\ \sum_{\ell=1}^L |\mathbf{c}_k^H \mathbf{F} \mathbf{w}_{j(\ell)}|_1 |s_{\ell}|_{\infty} &\leq \max_{\ell \in [L']} |\mathbf{c}_k^H \mathbf{F} \mathbf{w}_{\ell}|_1 \sum_{\ell=1}^L |s_{\ell}|_{\infty}. \quad (31) \end{aligned}$$

In (31), a) follows from the triangular inequality, and b) from Young's convolution inequality. We can now substitute the max argument on the right-hand side of (30) with the right-hand side of (31), and square the resulting expression as:

$$\begin{aligned} r_{\text{fs}}^2 &\leq \gamma^2 \max_{k \in [K'], \ell \in [L']} |\mathbf{c}_k^H \mathbf{F} \mathbf{w}_{\ell}|_1^2 \left(\sum_{\ell=1}^L |s_{\ell}|_{\infty} \right)^2 \stackrel{\text{a)}}{=} \\ \gamma^2 \mathbf{m}_{\mathbf{F}}^2(\mathbf{C}, \mathbf{W}) \left(\sum_{\ell=1}^L |s_{\ell}|_{\infty} \right)^2 &\stackrel{\text{b)}}{=} \\ \gamma^2 \mathbf{m}_{\mathbf{F}}^2(\mathbf{C}, \mathbf{W}) \left(\sum_{\ell=1}^L |s_{\ell}|_2 \sqrt{\rho_{s_{\ell}}/T} \right)^2 &\stackrel{\text{c)}}{\leq} \quad (32) \\ \gamma^2 \mathbf{m}_{\mathbf{F}}^2(\mathbf{C}, \mathbf{W}) \sum_{\ell=1}^L |s_{\ell}|_2^2 \sum_{\ell=1}^L \rho_{s_{\ell}}/T &\stackrel{\text{d)}}{=} \\ \gamma^2 \mathbf{m}_{\mathbf{F}}^2(\mathbf{C}, \mathbf{W}) P_{\text{tx}} \sum_{\ell=1}^L \rho_{s_{\ell}}. \end{aligned}$$

Here we have applied a) the definition of the max. SI in (5), b) (20), c) the Cauchy-Schwarz inequality, and d) (19). The proof is completed by substituting r_{fs}^2 in (29) with the right-hand side of (32) and rearranging.

ACKNOWLEDGMENT

The authors of this work acknowledge the financial support by the Federal Ministry of Education and Research of Germany (BMBF) in the programme ‘‘Souverän. Digital. Vernetzt.’’ Joint project 6G-RIC (grant numbers: 16KISK020K,

16KISK030). Rodrigo Hernangómez acknowledges BMBF support in the project ‘‘KOMSENS-6G’’ (grant number: 16KISK121).

REFERENCES

- [1] J. A. Zhang, M. L. Rahman, K. Wu, X. Huang, Y. J. Guo, S. Chen, and J. Yuan, ‘‘Enabling Joint Communication and Radar Sensing in Mobile Networks—A Survey,’’ *IEEE Communications Surveys Tutorials*, vol. 24, no. 1, pp. 306–345, 2022.
- [2] F. Liu, C. Masouros, A. P. Petropulu, H. Griffiths, and L. Hanzo, ‘‘Joint Radar and Communication Design: Applications, State-of-the-Art, and the Road Ahead,’’ *IEEE Transactions on Communications*, vol. 68, no. 6, pp. 3834–3862, Jun. 2020.
- [3] H. Wymeersch, A. Pärssinen, T. E. Abrudan, A. Wolfgang, K. Haneda, M. Sarajlic, M. E. Leinonen, M. F. Keskin, H. Chen, S. Lindberg, P. Kyösti, T. Svensson, and X. Yang, ‘‘6G Radio Requirements to Support Integrated Communication, Localization, and Sensing,’’ in *2022 Joint European Conference on Networks and Communications & 6G Summit (EuCNC/6G Summit)*, Jun. 2022, pp. 463–469.
- [4] F. Liu, Y. Cui, C. Masouros, J. Xu, T. X. Han, Y. C. Eldar, and S. Buzzi, ‘‘Integrated Sensing and Communications: Toward Dual-Functional Wireless Networks for 6G and Beyond,’’ *IEEE Journal on Selected Areas in Communications*, vol. 40, no. 6, pp. 1728–1767, Jun. 2022. [Online]. Available: <https://ieeexplore.ieee.org/document/9737357/>
- [5] C. Baquero Barneto, T. Riihonen, M. Turunen, L. Anttila, M. Fleischer, K. Stadius, J. Ryyanen, and M. Valkama, ‘‘Full-Duplex OFDM Radar With LTE and 5G NR Waveforms: Challenges, Solutions, and Measurements,’’ *IEEE Transactions on Microwave Theory and Techniques*, vol. 67, no. 10, pp. 4042–4054, Oct. 2019. [Online]. Available: <https://ieeexplore.ieee.org/document/8805161/>
- [6] L. Giroto de Oliveira, B. Nuss, M. B. Alabd, A. Diewald, M. Pauli, and T. Zwick, ‘‘Joint Radar-Communication Systems: Modulation Schemes and System Design,’’ *IEEE Transactions on Microwave Theory and Techniques*, vol. 70, no. 3, pp. 1521–1551, Mar. 2022. [Online]. Available: <https://ieeexplore.ieee.org/abstract/document/9627227>
- [7] M. A. Richards, J. A. Scheer, and W. A. Holm, *Principles of modern radar*. Raleigh (N.C.): Citeseer, 2010, vol. 1.
- [8] G. C. Alexandropoulos, M. A. Islam, and B. Smida, ‘‘Full-Duplex Massive Multiple-Input, Multiple-Output Architectures: Recent Advances, Applications, and Future Directions,’’ *IEEE Vehicular Technology Magazine*, vol. 17, no. 4, pp. 83–91, Dec. 2022. [Online]. Available: <https://ieeexplore.ieee.org/abstract/document/9933358>
- [9] R. Askar and W. Keusgen, ‘‘Lossless Decoupling Networks for RF Self-Interference Cancellation in MIMO Full-Duplex Transceivers,’’ *IEEE Journal on Selected Areas in Communications*, vol. 41, no. 9, pp. 2765–2779, Sep. 2023. [Online]. Available: <https://ieeexplore.ieee.org/abstract/document/10186241>
- [10] B. Smida, G. C. Alexandropoulos, T. Riihonen, and M. A. Islam, ‘‘In-Band Full-Duplex Multiple-Input Multiple-Output Systems for Simultaneous Communications and Sensing: Challenges, methods, and future perspectives,’’ *IEEE Signal Processing Magazine*, vol. 41, no. 5, pp. 8–16, Sep. 2024. [Online]. Available: <https://ieeexplore.ieee.org/abstract/document/10769781>
- [11] Z. He, W. Xu, H. Shen, D. W. K. Ng, Y. C. Eldar, and X. You, ‘‘Full-Duplex Communication for ISAC: Joint Beamforming and Power Optimization,’’ *IEEE Journal on Selected Areas in Communications*, vol. 41, no. 9, pp. 2920–2936, Sep. 2023.
- [12] A. Liu, T. Riihonen, and W. Sheng, ‘‘Full-Duplex Analog Beamforming Design for mm-Wave Integrated Sensing and Communication,’’ in *2023 IEEE Radar Conference (RadarConf23)*. San Antonio, TX, USA: IEEE, May 2023, pp. 1–6.
- [13] R. Hernangómez, J. Fink, R. L. Cavalcante, Z. Utkovski, and S. Stanczak, ‘‘Optimized Detection with Analog Beamforming for Monostatic Integrated Sensing and Communication,’’ in *ICC 2024 - IEEE International Conference on Communications*, Denver, CO, Jun. 2024, pp. 317–323. [Online]. Available: <https://ieeexplore.ieee.org/abstract/document/10622845>
- [14] I. P. Roberts, S. Vishwanath, and J. G. Andrews, ‘‘LoneSTAR: Analog Beamforming Codebooks for Full-Duplex Millimeter Wave Systems,’’ *IEEE Transactions on Wireless Communications*, vol. 22, no. 9, pp. 5754–5769, Sep. 2023. [Online]. Available: <https://ieeexplore.ieee.org/abstract/document/10022041>

- [15] M. Bayraktar, C. Rusu, N. González-Prelcic, and H. Chen, "Self-Interference Aware Codebook Design for Full-Duplex Joint Sensing and Communication Systems at Mmwave," in *2023 IEEE 9th International Workshop on Computational Advances in Multi-Sensor Adaptive Processing (CAMSAP)*, Dec. 2023, pp. 231–235. [Online]. Available: <https://ieeexplore.ieee.org/abstract/document/10403422>
- [16] M. Bayraktar, N. González-Prelcic, and H. Chen, "Hybrid Precoding and Combining for mmWave Full-Duplex Joint Radar and Communication Systems Under Self-Interference," in *ICC 2024 - IEEE International Conference on Communications*, Jun. 2024, pp. 915–920. [Online]. Available: <https://ieeexplore.ieee.org/abstract/document/10622490>
- [17] Z. Liu, S. Aditya, H. Li, and B. Clerckx, "Joint Transmit and Receive Beamforming Design in Full-Duplex Integrated Sensing and Communications," *IEEE Journal on Selected Areas in Communications*, vol. 41, no. 9, pp. 2907–2919, Sep. 2023.
- [18] E. Tohidi, R. Askar, Z. Utkovski, and S. Stańczak, "Full-duplex operation of ISAC: Self-interference reduction from the lens of IRS," in *2023 IEEE Globecom Workshops (GC Wkshps)*. IEEE, 2023, pp. 1880–1885. [Online]. Available: <https://ieeexplore.ieee.org/abstract/document/10464418/>
- [19] E. Dahlman, S. Parkvall, and J. Skold, *5G NR: The Next Generation Wireless Access Technology*, 1st ed. London England ; San Diego, CA: Academic Press, Aug. 2018.
- [20] R. Askar, J. Chung, Z. Guo, H. Ko, W. Keusgen, and T. Haustein, "Interference Handling Challenges toward Full Duplex Evolution in 5G and Beyond Cellular Networks," *IEEE Wireless Communications*, vol. 28, no. 1, pp. 51–59, Feb. 2021. [Online]. Available: <https://ieeexplore.ieee.org/abstract/document/9363023>
- [21] Y. He, X. Yin, and H. Chen, "Spatiotemporal characterization of self-interference channels for 60-GHz full-duplex communication," *IEEE Antennas and Wireless Propagation Letters*, vol. 16, pp. 2220–2223, 2017. [Online]. Available: <https://ieeexplore.ieee.org/abstract/document/7932916>
- [22] S. Mandelli, M. Henninger, M. Bauhofer, and T. Wild, "Survey on Integrated Sensing and Communication Performance Modeling and Use Cases Feasibility," in *2023 2nd International Conference on 6G Networking (6GNet)*, Oct. 2023, pp. 1–8. [Online]. Available: <https://ieeexplore.ieee.org/abstract/document/10317691>
- [23] B. Fuchs, "Application of Convex Relaxation to Array Synthesis Problems," *IEEE Transactions on Antennas and Propagation*, vol. 62, no. 2, pp. 634–640, Feb. 2014. [Online]. Available: <https://ieeexplore.ieee.org/abstract/document/6663667>
- [24] J. Hoydis, S. Cammerer, F. Ait Aoudia, A. Vem, N. Binder, G. Marcus, and A. Keller, "Sionna: An open-source library for next-generation physical layer research," *arXiv preprint*, Mar. 2022. [Online]. Available: <https://arxiv.org/abs/2203.11854>
- [25] G. Sagnol, "A class of semidefinite programs with rank-one solutions," *Linear Algebra and its Applications*, vol. 435, no. 6, pp. 1446–1463, Sep. 2011. [Online]. Available: <https://linkinghub.elsevier.com/retrieve/pii/S0024379511002515>
- [26] R. Gray, "Quantization noise spectra," *IEEE Transactions on Information Theory*, vol. 36, no. 6, pp. 1220–1244, Nov. 1990. [Online]. Available: <https://ieeexplore.ieee.org/abstract/document/59924>
- [27] E. Hewitt and K. A. Ross, *Abstract Harmonic Analysis: Volume I: Structure of Topological Groups Integration Theory Group Representations*. Springer Science & Business Media, Dec. 2012.
- [28] 3GPP, "Study on channel model for frequencies from 0.5 to 100 GHz," TR 38.901, Release 16.1, Nov. 2020.
- [29] D. Dehghani, "Analog Beamforming Simulations for Self-Interference Cancellation in Integrated Sensing and Communication (ISAC)," Master's thesis, Karlsruhe Institute of Technology, Karlsruhe, Germany, Jun. 2024.
- [30] S. Diamond and S. Boyd, "CVXPY: A Python-embedded modeling language for convex optimization," *Journal of Machine Learning Research*, vol. 17, no. 83, pp. 1–5, 2016.
- [31] X. Wang, "A Simple Proof of Descartes's Rule of Signs," *The American Mathematical Monthly*, vol. 111, no. 6, pp. 525–526, Jun. 2004. [Online]. Available: <https://doi.org/10.1080/00029890.2004.11920108>